Astronomy & Astrophysics manuscript no. art49a February 2, 2008
(DOI: will be inserted by hand later)

Long Period Variables in the Magellanic Clouds: OGLE + 2MASS + DENIS ⋆

M.A.T. Groenewegen

Instituut voor Sterrenkunde, K.U. Leuven, PACS-ICC, Celestijnenlaan 200B, B–3001 Leuven, Belgium

received: 2004, accepted: 2004

Abstract. The 68 000 I-band light curves of variable stars detected by the OGLE survey in the Large and Small Magellanic Clouds (MCs) are fitted by Fourier series, and also correlated with the DENIS and 2MASS *all-sky release* databases and with lists of spectroscopically confirmed M-, S- and C-stars. Lightcurves and the results of the lightcurve fitting (periods and amplitudes) and DENIS and 2MASS magnitudes are presented for 2277 M-,S-,C-stars in the MCs. The following aspects are discussed: the K-band period-luminosity relations for the spectroscopically confirmed AGB stars, period changes over a timespan of about 17 years in a subset of about 400 LPVs, and candidate obscured AGB stars. The use of a sample of spectroscopically confirmed variables allows me to show specifically that almost all carbon stars are brighter than the tip of the RGB, and occupy sequences A+,B+,C and D. It is shown (for the LMC where there is a sufficient number of spectroscopically identified M-stars) that for sequences A+,B+,C the M-stars are on average fainter than the C-stars, as expected from an evolutionary point of view and previously observed in MC clusters. However, this is not so for sequence "D", suggesting that the origin of the so-called Long Secondary Periods is not related to an evolutionary effect. The fraction of objects that has a period on sequence "D" is also independent of chemical type. Three stars are identified that have been classified as oxygen-rich in the 1970s and carbon-rich in 1990s. Possibly they underwent a thermal pulse in the last 20 years, and dredged-up enough carbon to switch spectral type. The observations over almost two decades seem to suggest that up to 10% of AGB variables changed pulsation mode over that time span. More robust estimates will come from the ongoing and future (microlensing) photometric surveys. A sample of 570 variable red objects ($(J-K) > 2.0$ or $(I-K) > 4.0$) is presented in which most stars are expected to be dust obscured AGB stars. Estimates are presented for cut-offs in $(J-K)$ which should be applied to minimise dust obscuration in K, and based on this, C- and O-star K-band PL-relations for large amplitude variables in the SMC and LMC are presented.

Key words. Stars: AGB and post-AGB - Stars: carbon - Stars: variables: general - Magellanic Clouds

1. Introduction

In the course of the micro lensing surveys in the 1990's, the monitoring of the Small and Large Magellanic Clouds has revealed an amazing number and variety of variable stars. A big impact was felt and is being felt in many areas of variable star research, like Cepheids and RR Lyrae stars. Also in the area of Long Period Variables (LPVs) and AGB stars there has been remarkable progress. Wood et al. (1999) and Wood (2000) were the first to identify and label different sequences "ABC" thought to represent the classical Mira sequence ("C") and overtone pulsators ("A,B"), and sequence "D" which is still unexplained (Olivier & Wood 2003, Wood 2003, 2004). Stars on these sequence are sometimes referred to as having Long Secondary Periods–LSPs. This view has subsequently been confirmed and expanded upon by Noda et al. (2002), Lebzelter et al. (2002), Cioni et al. (2003), Ita et al. (2004a,b) and Kiss & Bedding (2003, 2004). These works differ in the source of the variability data (MACHO, OGLE, EROS, MOA), area (SMC or LMC), associated infrared data (Siding Spring 2.3m, DENIS, 2MASS, SIRIUS), and selection on pulsation amplitude or infrared colours.

The present paper considers the OGLE data for both LMC and SMC. Ita et al. (2004a) only consider the OGLE data in overlap with their SIRIUS IR observations in LMC and SMC, and Kiss & Bedding consider only stars in the SMC with 2MASS data with $(J-K) > 0.9$.

Also in contrast to previous studies, emphasis is put on spectroscopically confirmed AGB stars (i.e. M-, S- and C-stars). In other studies M- and C-stars are usually identified photometrically by using a division at a $(J-K)$ colour of $\sim$1.4 mag. This paper specifically addresses the properties of known carbon stars in relation to sequences "ABCD".

The paper is structured as follows. In Section 2 the OGLE, 2MASS and DENIS surveys are described. In Section 3 the model is presented, both in terms of the actual lightcurve fit-

Send offprint requests to: Martin Groenewegen (groen@ster.kuleuven.ac.be)

⋆ Tables 2, 3, 6, 7 and 8 are available in electronic form at the CDS via anonymous ftp to cdsarc.u-strasbg.fr (130.79.128.5) or via http://cdsweb.u-strasbg.fr/cgi-bin/qcat?J/A+A/. Figures 2, 9 and 13 are available in the on-line edition of A&A.

ting, and the post-processing. Section 4 presents the results. Discussed are the K-band PL-relation for the spectroscopically confirmed AGB stars, period changes over a timespan of almost 2 decades, and a sample of very red obscured AGB star candidates. The conclusions are summarised in Section 5. Some of this work, and the star-to-star comparison of periods derived by me from MACHO and OGLE data and literature values are described in Groenewegen (2004).

2. The data sets

Zebruń et al. (2001) describe the dataset of the about 68 000 variable objects detected by OGLE in the direction of the LMC and SMC, obtained in the course of the OGLE-II micro lensing survey using the difference image analysis (DIA) technique. Twenty-one fields in the central parts of the LMC, and 11 fields in the central parts of the SMC of size $14.2' \times 57'$ each were observed in BVI, with an absolute photometric accuracy of 0.01-0.02 mag. The large majority of data was obtained in the I-band (and the DIA analysis has been done only on the I-band data), and these data were downloaded from the OGLE homepage (http://sirius.astrouw.edu.pl/~ogle/).

The DENIS survey is a survey of the southern hemisphere in $IJK_{\rm s}$ (Epchtein et al. 1999). Cioni et al. (2000) describe a point source catalog of sources in the direction of the Magellanic Clouds (MCs; DCMC = DENIS Catalogue towards the Magellanic Clouds) containing 1 635 680 objects with a detection in at least 2 of the 3 photometric bands that is available in electronic form. The 68193 OGLE objects were correlated on position using a $3''$ search radius and 40793 matches were found.

The 2MASS survey is an all-sky survey in the $JHK_{\rm s}$ near-infrared bands. On March 25, 2003 the 2MASS team released the all-sky point source catalog. The easiest way to check if a star is included in the 2MASS database is by uplinking a source table with coordinates to the 2MASS homepage. Such a table was prepared for the 68193 OGLE objects and correlated on position using a $3''$ radius. Data on 50129 objects were returned.

3. The model

At the heart of the data processing are two numerical codes, that are described in detail in the Appendices. Briefly, the first code (see for details Appendix A) sequentially reads in the I-band data for the 68 000 objects, determines periods through Fourier analysis, fits sine and cosine functions to the light curve through linear least-squares fitting and makes the final correlation with the pre-prepared DENIS and 2MASS source lists. All the relevant output quantities are written to file.

This file is read in by the second code (see for details Appendix B). A further selection may be applied (typically on period, amplitude and mean I-magnitude), multiple entries are filtered out (i.e. objects that appear in different OGLE fields), and a correlation is made with pre-prepared lists of known non-LPVs and known LPVs or AGB stars. The output of the second code is a list with LPV candidates.

The third step (for details see Appendix C) consists of a visual inspection of the fits to the light curves of the candidate LPVs and a literature study through a correlation with the SIMBAD database. Non-LPVs are removed, and sometimes the fitting is redone. The final list of LPV candidates is compiled.

fig1.jpg

Fig. 1. Difference in photometry, *after* the following offsets have been applied: I(denis-ogle) = -0.018, J(denis-2mass)= -0.090, K(denis-2mass)= -0.14. Used in the analysis are the stars with an I-band amplitude < 0.05 mag. Plotted are about 12000, 8700, and 5700 stars, top to bottom.

4. Results

4.1. Astrometry

The spatial correlation between the OGLE objects and known LPVs and AGB stars, and known non-LPVs, is actually done in 2 steps. In the first step the correlation is made, and the differences and spread in ΔRA $\cos(\delta)$ and $\Delta\delta$ are determined. These mean offsets are then applied to make the final cross-correlation. The results are listed in Table 1. Regarding the MACHO data the agreement between the offsets determined from the list of non-LPVs, and the data by Wood et al. (1999) is good and a combined offset of Δ RA $\cos(\delta) = 0.52''$ and $\Delta\delta = 0.16''$ is applied. With respect to the other sources of astrometry, similar small changes have been found, and in most cases applied, usually increasing the number of matches in the final matching.

Table 1. Comparison of coordinates, and number of positional matches, before and after a correction was applied.

OGLE- (*other*)	Δ RA $\cos(\delta)$	$\Delta\delta$	N	Δ RA $\cos(\delta)$	$\Delta\delta$	N	remark
MACHO	0.52 ± 0.61	0.21 ± 0.63	647	0.06 ± 0.63	0.05 ± 0.64	662	mainly "blue objects" and EBs
MACHO	0.52 ± 1.28	0.14 ± 1.23	1427	0.11 ± 1.31	-0.02 ± 1.22	1436	LPVs; Wood et al. 1999
MOA	-0.01 ± 0.32	0.008 ± 0.55	123	–	–	–	EBs; no correction applied
MOA	0.78 ± 1.04	0.002 ± 0.94	150	0.11 ± 0.97	0.03 ± 0.94	150	LPVs; Noda et al. 2002
EROS	0.41 ± 0.50	-0.21 ± 0.48	368	0.06 ± 0.58	0.01 ± 0.49	381	cepheids and EBs
AGAPEROS	0.31 ± 1.09	0.37 ± 1.00	503	0.05 ± 1.07	0.05 ± 0.95	501	LPVs; Letzelter et al. 2002
DENIS	-0.10 ± 1.33	0.02 ± 1.37	313	–	–	–	LPVs; Cioni et al. 2003; no correction applied
HUGHES	2.19 ± 1.50	0.85 ± 1.41	433	0.22 ± 1.34	-0.01 ± 1.34	436	LPVs
KDM	0.55 ± 1.12	-0.23 ± 0.90	1024	0.06 ± 1.11	-0.03 ± 0.90	1028	carbon stars
RAW	-1.06 ± 0.80	1.03 ± 0.71	873	0.04 ± 0.76	0.04 ± 0.70	874	carbon stars
BMB	0.42 ± 0.90	0.00 ± 0.66	381	0.05 ± 0.96	-0.01 ± 0.68	385	AGB stars

Table 2. First entries in the electronically available table, which lists: OGLE-field, OGLE-name, the three fitted periods with errors and amplitude (0.00 means no fit), mean $I_{\rm ogle}$, and associated DENIS IJK photometry with errors, and associated 2MASS JHK photometry with errors (99.9 and 9.99 means no association, or no value).

Field	OGLE-name	Period	Amp	Period	Amp	Period	Amp	$I_{\rm ogle}$	$I_{\rm denis}$	$J_{\rm denis}$	$K_{\rm denis}$	$J_{\rm 2MASS}$	$H_{\rm 2MASS}$	$K_{\rm 2MASS}$
smc_sc1	OGLE003616.76-732132.7	95.2 ± 0.138	0.042	168.5 ± 0.335	0.064	771.7 ± 7.449	0.140	14.47	14.42 ± 0.01	12.66 ± 0.01	11.17 ± 0.02	12.79 ± 0.03	11.74 ± 0.03	11.27 ± 0.03
smc_sc1	OGLE003626.98-733704.3	57.8 ± 0.054	0.020	88.5 ± 0.142	0.018	730.4 ± 4.627	0.041	14.73	14.86 ± 0.02	13.38 ± 0.02	12.32 ± 0.06	13.48 ± 0.03	12.72 ± 0.03	12.34 ± 0.03
smc_sc1	OGLE003630.80-735456.4	0.0 ± 0.000	0.000	0.0 ± 0.000	0.000	0.0 ± 0.000	0.000	14.44	14.54 ± 0.01	13.09 ± 0.01	11.93 ± 0.05	13.20 ± 0.03	12.38 ± 0.03	12.12 ± 0.03
smc_sc1	OGLE003633.16-730547.6	83.9 ± 0.200	0.029	166.9 ± 0.393	0.057	0.0 ± 0.000	0.000	14.24	14.23 ± 0.01	12.68 ± 0.01	11.48 ± 0.03	12.78 ± 0.02	11.90 ± 0.03	11.55 ± 0.03
smc_sc1	OGLE003633.30-735040.6	135.3 ± 0.118	0.063	755.8 ± 1.033	0.195	0.0 ± 0.000	0.000	14.56	14.47 ± 0.01	12.89 ± 0.01	11.39 ± 0.03	13.00 ± 0.03	12.02 ± 0.03	11.52 ± 0.03
smc_sc1	OGLE003635.63-733551.9	113.8 ± 0.083	0.050	186.5 ± 0.420	0.027	727.8 ± 3.174	0.049	14.22	14.31 ± 0.01	12.59 ± 0.01	11.06 ± 0.02	12.72 ± 0.03	11.73 ± 0.03	11.18 ± 0.02
smc_sc1	OGLE003638.83-734635.4	179.2 ± 0.057	0.243	0.0 ± 0.000	0.000	0.0 ± 0.000	0.000	15.16	14.85 ± 0.02	13.13 ± 0.02	11.66 ± 0.04	13.26 ± 0.03	12.28 ± 0.03	11.74 ± 0.03
smc_sc1	OGLE003643.09-735018.3	107.5 ± 0.105	0.051	135.3 ± 0.198	0.043	1330.7 ± 14.439	0.102	14.21	14.07 ± 0.01	12.43 ± 0.01	11.12 ± 0.02	12.58 ± 0.02	11.67 ± 0.03	11.27 ± 0.03
smc_sc1	OGLE003646.48-734220.6	188.1 ± 0.377	0.035	281.8 ± 0.657	0.046	0.0 ± 0.000	0.000	14.30	14.22 ± 0.01	12.76 ± 0.01	11.68 ± 0.04	12.95 ± 0.03	12.13 ± 0.03	11.81 ± 0.03
smc_sc1	OGLE003649.80-730416.4	616.8 ± 12.389	0.011	0.0 ± 0.000	0.000	0.0 ± 0.000	0.000	14.52	14.66 ± 0.01	13.14 ± 0.01	11.94 ± 0.05	13.22 ± 0.03	12.41 ± 0.03	12.12 ± 0.03
smc_sc1	OGLE003650.09-731737.3	105.1 ± 0.040	0.090	251.8 ± 0.291	0.072	559.2 ± 1.585	0.070	14.14	14.19 ± 0.01	12.51 ± 0.01	11.28 ± 0.03	12.71 ± 0.03	11.80 ± 0.03	11.46 ± 0.02
smc_sc1	OGLE003651.78-732400.0	66.3 ± 0.070	0.018	0.0 ± 0.000	0.000	0.0 ± 0.000	0.000	14.53	14.62 ± 0.01	13.04 ± 0.01	11.78 ± 0.04	13.17 ± 0.03	12.29 ± 0.03	12.00 ± 0.03
smc_sc1	OGLE003653.17-733620.3	251.1 ± 0.970	0.021	0.0 ± 0.000	0.000	0.0 ± 0.000	0.000	14.15	14.22 ± 0.01	12.65 ± 0.01	11.36 ± 0.03	12.75 ± 0.02	11.87 ± 0.03	11.48 ± 0.02
smc_sc1	OGLE003700.95-731637.7	118.1 ± 0.064	0.065	222.2 ± 0.118	0.126	0.0 ± 0.000	0.000	14.42	14.51 ± 0.01	12.84 ± 0.01	11.45 ± 0.03	13.06 ± 0.03	12.06 ± 0.03	11.59 ± 0.03
smc_sc1	OGLE003703.93-735608.3	0.0 ± 0.000	0.000	0.0 ± 0.000	0.000	0.0 ± 0.000	0.000	15.28	99.00 ± 9.99	99.00 ± 9.99	99.00 ± 9.99	14.20 ± 0.04	13.44 ± 0.05	13.23 ± 0.06
smc_sc1	OGLE003705.38-734426.3	95.3 ± 0.049	0.061	189.9 ± 0.297	0.043	514.9 ± 2.064	0.056	14.72	14.78 ± 0.01	13.22 ± 0.01	11.56 ± 0.03	13.28 ± 0.04	99.00 ± 9.99	99.00 ± 9.99
smc_sc1	OGLE003712.83-731133.5	361.0 ± 1.652	0.104	481.1 ± 1.764	0.148	872.6 ± 2.103	0.315	14.27	14.13 ± 0.01	12.42 ± 0.01	10.81 ± 0.02	12.53 ± 0.03	11.45 ± 0.03	10.94 ± 0.03
smc_sc1	OGLE003716.26-732048.9	172.3 ± 0.218	0.052	216.8 ± 0.170	0.098	0.0 ± 0.000	0.000	14.39	14.66 ± 0.01	13.06 ± 0.02	11.62 ± 0.04	13.09 ± 0.02	12.15 ± 0.02	11.76 ± 0.03
smc_sc1	OGLE003718.97-735029.8	65.2 ± 0.102	0.011	603.8 ± 3.661	0.032	0.0 ± 0.000	0.000	14.26	14.29 ± 0.01	12.98 ± 0.01	11.81 ± 0.04	13.07 ± 0.02	12.26 ± 0.02	11.99 ± 0.02
smc_sc1	OGLE003722.15-732222.8	102.0 ± 0.101	0.033	342.2 ± 0.527	0.100	684.9 ± 0.902	0.274	14.36	14.77 ± 0.01	13.12 ± 0.02	11.60 ± 0.03	13.28 ± 0.02	12.23 ± 0.02	11.76 ± 0.03
smc_sc1	OGLE003726.67-731710.4	646.7 ± 6.002	0.023	0.0 ± 0.000	0.000	0.0 ± 0.000	0.000	14.71	14.75 ± 0.01	13.24 ± 0.02	12.15 ± 0.06	13.35 ± 0.03	12.51 ± 0.03	12.24 ± 0.02
smc_sc1	OGLE003734.50-732110.6	120.1 ± 0.150	0.056	131.3 ± 0.158	0.063	328.7 ± 0.541	0.063	14.61	99.00 ± 9.99	99.00 ± 9.99	99.00 ± 9.99	13.10 ± 0.03	12.08 ± 0.02	11.66 ± 0.02
smc_sc1	OGLE003735.61-730421.6	171.2 ± 0.486	0.023	243.0 ± 0.773	0.028	542.5 ± 6.147	0.019	14.19	99.00 ± 9.99	99.00 ± 9.99	99.00 ± 9.99	12.71 ± 0.03	11.73 ± 0.02	11.32 ± 0.02

Table 3. First entries in the electronically available table, which list: OGLE-field, OGLE-name, other names, spectral type and references and comments.

Field	OGLE-name	Other Name	SpT	Comments
smc_sc1	OGLE003616.76-732132.7	MH_0344	C	
smc_sc1	OGLE003626.98-733704.3	MH_0349	C	
smc_sc1	OGLE003630.80-735456.4	MH_0352	C	
smc_sc1	OGLE003633.16-730547.6	RAW_0003	C	
smc_sc1	OGLE003633.30-735040.6	MH_0354	C	
smc_sc1	OGLE003635.63-733551.9	RAW_0004	C	
smc_sc1	OGLE003638.83-734635.4	MH_0358	C	
smc_sc1	OGLE003643.09-735018.3	MH_0361	C	
smc_sc1	OGLE003646.48-734220.6	RAW_0005	C	
smc_sc1	OGLE003649.80-730416.4	RAW_0007	C	
smc_sc1	OGLE003650.09-731737.3	RAW_0008	C	
smc_sc1	OGLE003651.78-732400.0	RAW_0009	C	
smc_sc1	OGLE003653.17-733620.3	RAW_0010	C	
smc_sc1	OGLE003700.95-731637.7	RAW_0011	C	
smc_sc1	OGLE003703.93-735608.3	MH_0370	C	
smc_sc1	OGLE003705.38-734426.3	MH_0371	C	
smc_sc1	OGLE003712.83-731133.5	RAW_0012	C	
smc_sc1	OGLE003716.26-732048.9	RAW_0013	C	
smc_sc1	OGLE003718.97-735029.8	MH_0374	C	
smc_sc1	OGLE003722.15-732222.8	RAW_0014	C	
smc_sc1	OGLE003726.67-731710.4	RAW_0015	C	
smc_sc1	OGLE003734.50-732110.6	RAW_0016	C	
smc_sc1	OGLE003735.61-730421.6	RAW_0017	C	

4.2. Photometry

As was already discussed in Groenewegen (2004), by selecting the least variable stars in the OGLE database one can compare photometry.

In particular the OGLE I was compared to the (singe-epoch) DENIS I, and the (single-epoch) DENIS JK was compared to the (single-epoch) 2MASS JK magnitudes. This was done by selecting those objects with an amplitude in the I-band of < 0.05 mag.

Figure 1 shows the final results when offsets I(denis-ogle) = -0.018, J(denis-2mass)= -0.090, and K(denis-2mass)= -0.14 are applied. The offsets derived here are very similar to those derived in Delmotte et al. (2002) using a similar analysis based on a direct comparison of DENIS with the 2MASS 2nd incremental data-release (they found: J(denis-2mass) = -0.11 ± 0.06, and K(denis-2mass)= -0.14 ± 0.06).

4.3. The sample of spectroscopically confirmed M,S,C-stars

As mentioned before, a correlation was made with a list that contains 12631 objects over the entire MCs with a spectroscopically determined spectral type. Using a $4''$ search radius, 2478 unique objects were found in the OGLE fields. After visual in-

spection (removing mostly obviously incorrect positional mismatches, indicated by association with very faint OGLE objects with hardly any variability [sect. 3.2.2]) there remain 2277 objects (856 C- and 3 M-stars in the SMC, 1064 C-, 10 S-, 344 M-stars in the LMC) which are the subject of further study. Their lightcurves are shown in Figure 2 (only the first few, the full figure only being available in the electronic edition), the results of the lightcurve analysis and association with DENIS and 2MASS is given in Table 2, and the association with known objects and additional comments and references are given in Table 3 (again, only the first few entries are shown, the full tables being available only electronically).

In the discussion that follows, magnitudes are dereddened using the $A_{\rm V}$ values that correspond to the respective OGLE field in the SMC or LMC, and selective reddenings of $A_{\rm I}/A_{\rm V} = 0.49$, $A_{\rm J}/A_{\rm V} = 0.27$, $A_{\rm H}/A_{\rm V} = 0.20$, $A_{\rm K}/A_{\rm V} = 0.12$ (Draine 2003) are used.

Some of the objects have different spectral classifications in different surveys. These have been identified in Table 3. Some of them are in fact due to a typographical error in CML (Cioni, private communication). In all other cases the different sources of photometry, pulsation periods (when available) and close proximity suggest that these objects are one and the same. For one object, OGLE052711.00-692827.5, both associated objects have an uncertain spectral type: WBP-48 is classified as (M?), SHV052733.4-693050 as (CS?). It is kept as "M". OGLE052705.07-693606.9 is associated with the carbon star KDM-4094, but also with the M-star HV 12048, and the latter type is assumed here. Of course oxygen-rich stars may evolve into carbon-rich stars, and three more objects that may have evolved in this way judging from the different spectral types are OGLE050859.83-691458.0 (WOH-G-202, KDM-2226), OGLE054109.00-700942.1 (WOH-G-473, KDM-5626), and OGLE054120.38-700823.3 (WOH-G-478, KDM-5645). In all cases the more recent spectral type (C) has been adopted. These stars are valid targets for spectroscopy, both in the optical to determine their (s-process) abundances, and in the mid-infrared to identify the dust features of the possibly still oxygen-rich dust shell.

Six objects are erroneously associated by SIMBAD with relatively bright objects, and an appropriate comment is added in Table 3. The alledged counterparts have B and/or V magnitudes in the range 10-13 mag, while the $I_{\rm ogle}$, and the photoelectric R and I magnitude (all six objects happen to be listed in KDM) are typically 14-15 mag and suggest B, V magnitudes that would be closer to 16-18 mag. Optical and 2MASS finding charts were also inspected and a bright object was typically found within $1'$ of the OGLE object.

One of the major finding by Wood et al. (1999), Wood (2000) and subsequently confirmed by other studies is the existence of distinct PL-relations, usually indicated by the letters A-,A+,B-,B+,C,D. The values for the boundaries of these regions were originally taken from Ita et al. (2004a), Ita (private communication) and then slightly adapted. They are basically drawn by eye, and for reference the lines that define the boundaries have been listed in Table 4. The boundaries between A- and A+, and B- and B+, are placed at the tip of the RGB, i.e. K_0 = 12.1, and 12.7 in the LMC and SMC, respectively.

Figure 3 shows the PL-relation in the K-band with these boundaries, for the SMC and LMC separately, and according to cuts in the I-band amplitude, as indicated in the insets. The K-band is on the 2MASS system, and is the average of the DENIS and 2MASS photometry. In particular, if both DENIS and 2MASS K-band data is available, the DENIS data point is corrected as explained above (i.e. 0.14 mag added), and averaged with the 2MASS data point. This should take out some of the scatter in the PL-diagram, as the effect of the variability in the K-band is reduced. If only DENIS is available, the corrected value is used. Not all periods listed in Table 2 are plotted. Inspecting the outliers in preliminary versions of Figure 3 indicated that to reduce the scatter a further culling was necessary, in particular at the longer periods, as the timespan of the OGLE observations is about 1100 days. The following conditions were applied (with ΔP the error in the period): $\Delta P/P < 0.01$ for $P < 500^d$; $\Delta P < 5^d$ for $500^d < P < 800^d$ and $\Delta P < 1.5^d$ for $P > 800^d$. Figures 3, 4, 5, 6, 7, 10, 12, 14 and all calculations are based on periods that obey these conditions. In contrast, all periods found have been listed in Tables 2 and 7 and are shown in Figures 2, 9 and 13.

The following systematics may be observed: (1) small amplitude variables are present at all periods, (2) objects with I-band amplitudes $\gtrsim$0.05 are not found in box "A+" (nor "A-"), (3) objects with I-band amplitudes $\gtrsim$0.45 are mainly found in box "C". These three remarks are valid for SMC and LMC alike.

Unfortunately, only three confirmed oxygen-rich SMC stars appear in Tables 2 and 3, and all come from an IRAS selected sample (GB98). They all have (very) long periods and the error in these periods are such that only one period appears in Figure 3.

For the LMC the situation is better. One can observe that: (4) essentially all SMC, and almost all LMC, carbon stars are brighter than the tip of the RGB, (5) LMC M-stars are observed below the TRGB, but only at small amplitudes, (6) for a given "box" or amplitude cut, the M-stars are on average fainter than the C-stars, (7) a few stars brighter than the expected tip of the AGB, presumably supergiants, are present, and they predominantly have large pulsation amplitudes.

Statement 6 is illustrated in more detail in Figures 4 and 5, where, respectively, LMC and SMC K-band histograms are shown for the stars inside different "boxes" and partly for different I-band amplitude cuts, as indicated in the insets. For the LMC a distinction is made between C- and M/S-stars and for sequences A+,B+ and C the M-stars are on average fainter than the C-stars. The seems not to be the case for sequence D, suggesting that the LSP phenomenon is not related to evolutionary status.

Figure 6 shows the Amplitude-Period diagram for LMC and SMC. They look qualitatively similar, and similar to diagrams shown in Ita et al. (2004a) and Cioni et al. (2003). Interestingly, it appears that for a given amplitude, the LMC M-stars have on average shorter periods than the C-stars. This is a different manifestation of something that could already be seen in Figure 3, most clearly in the panel with the cut $0.15 \leq$ Amplitude < 0.45 where sequence "B+" contains mainly M-stars while sequence "C" contains mainly C-stars.

Fig. 2. First entries of electronically available figure with all lightcurves. The fit is indicated by the (red) solid line. Crosses indicate data points not included in the fit.

Table 4. Definition of the boundary lines of the sequences in the K-band PL-diagram in Figure 3. Relations are of the form $K_{\rm min,max} = {\rm slope}_{\rm min,max} \log P + {\rm zp}_{\rm min,max}$, with K the dereddened magnitude on the 2MASS system.

	$K_{\rm max}$	$K_{\rm min}$	slope$_{\rm min}$	zp$_{\rm min}$	slope$_{\rm max}$	zp$_{\rm max}$	comment
				SMC			
A-	12.7	13.5	-3.35	17.23	-3.35	17.85	slope from Ita (priv. comm.)
A+	10.0	12.7	-3.45	17.10	-3.45	17.85	slope from Ita (priv. comm.)
B-	12.7	13.5	-3.35	17.85	-3.35	18.77	slope from Ita (priv. comm.)
B+	10.0	12.7	-3.45	17.95	-3.45	19.00	slope from Ita (priv. comm.)
C	10.0	12.7	-3.85	20.05	-3.85	21.45	slope from Ita (priv. comm.)
D	10.5	13.0	-3.85	21.55	-3.85	23.50	slope from Ita (priv. comm.)
				LMC			
A-	12.1	13.5	-3.35	16.70	-3.35	17.50	slope from Ita (priv. comm.)
A+	9.4	12.1	-3.45	16.50	-4.00	18.45	
B-	12.1	13.5	-3.35	17.50	-3.35	18.50	slope from Ita (priv. comm.)
B+	9.4	12.1	-4.00	18.55	-4.00	19.80	
C	9.4	12.5	-3.80	19.50	-3.80	20.90	
D	9.8	13.0	-3.85	21.20	-3.85	23.90	slope from Ita (priv. comm.)

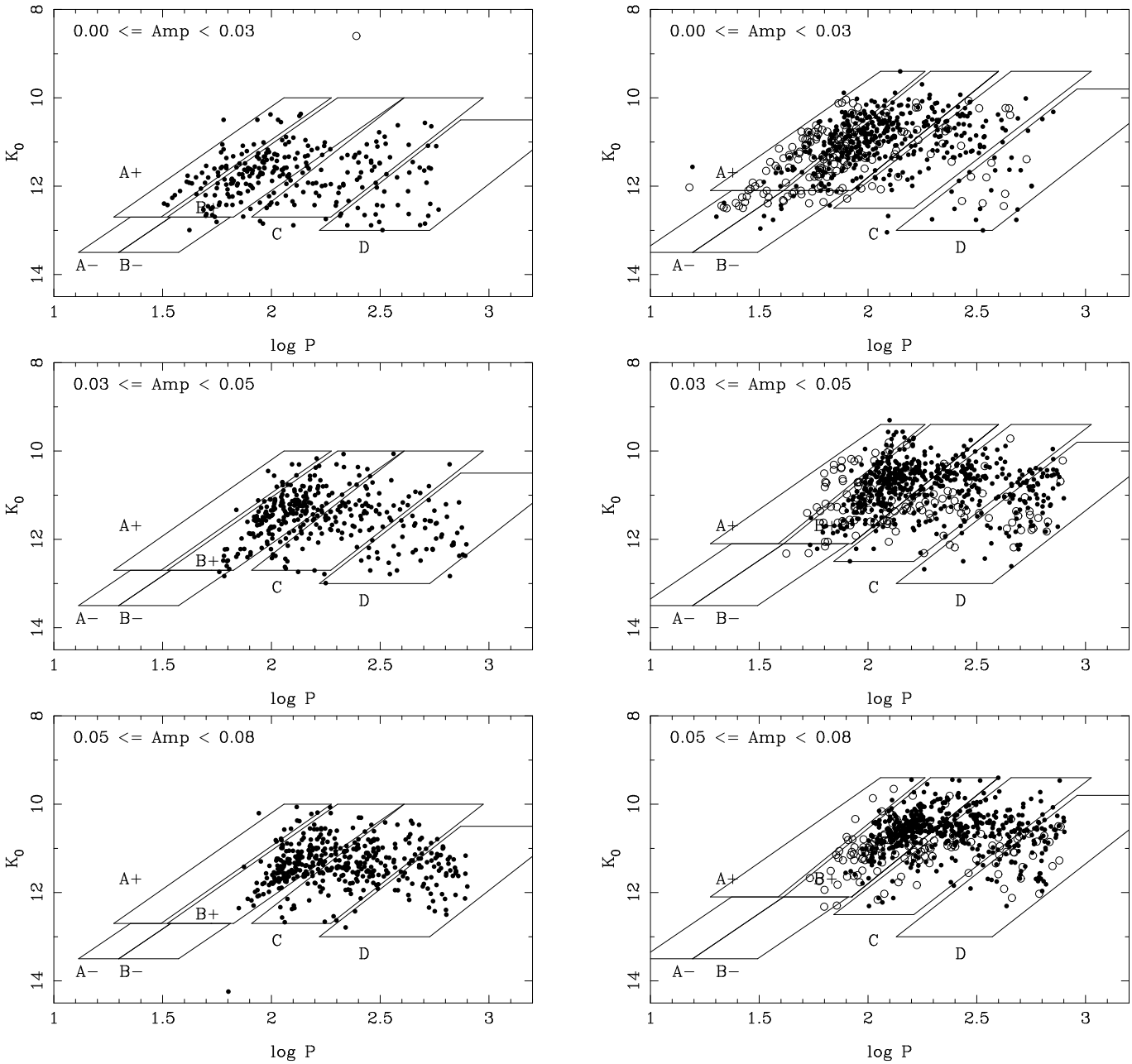

Fig. 3. K-band PL-relation, for the SMC (left) and LMC (right). Panles indicate selection on I-band amplitude. Carbon stars are indicated by filled circels, M- and S-stars by open circels. All periods from Table 2 that fulfil $\Delta P/P < 0.01$ for $P < 500^d$; $\Delta P < 5^d$ for $500^d < P < 800^d$ and $\Delta P < 1.5^d$ for $P > 800^d$ are plotted. Boxes related to the "ABCD" sequences are indicated. The functional dependence is summarised in Table 4.

Figure 7 shows the Period-Colour diagram for LMC and SMC for DENIS and 2MASS data. They look qualitatively similar to diagrams shown in Lebzelter et al. (2002) and Ita et al. (2004a). Two features may be remarked upon, (1) there are more red carbon stars in the LMC than in the SMC (at least that are spectroscopically confirmed), (2) The M-stars are much more spread in $(I-J)_0$ than in $(J-K)_0$ colour.

The first observation may be related to an, on average, higher mass loss rate of AGB stars in the LMC compared to the SMC. Section 4.5 deals in more detail with obscured objects. The second observation is a known effect and related to the strong temperature dependence of the molecular bands in the red part of the optical spectrum in M-stars. Table 5 lists the $(I-J)$ and $(J-K)$ colours according to the model atmospheres (for solar metallicity) of M-stars (Fluks et al. 1994), and carbon stars (Loidl et al. 2001, her model with a C/O ratio of 1.1). In addition, for a few selected models the colours are listed in the last column of the stars when obscured by 0.05 magnitudes in K by dust (see Section 4.5).

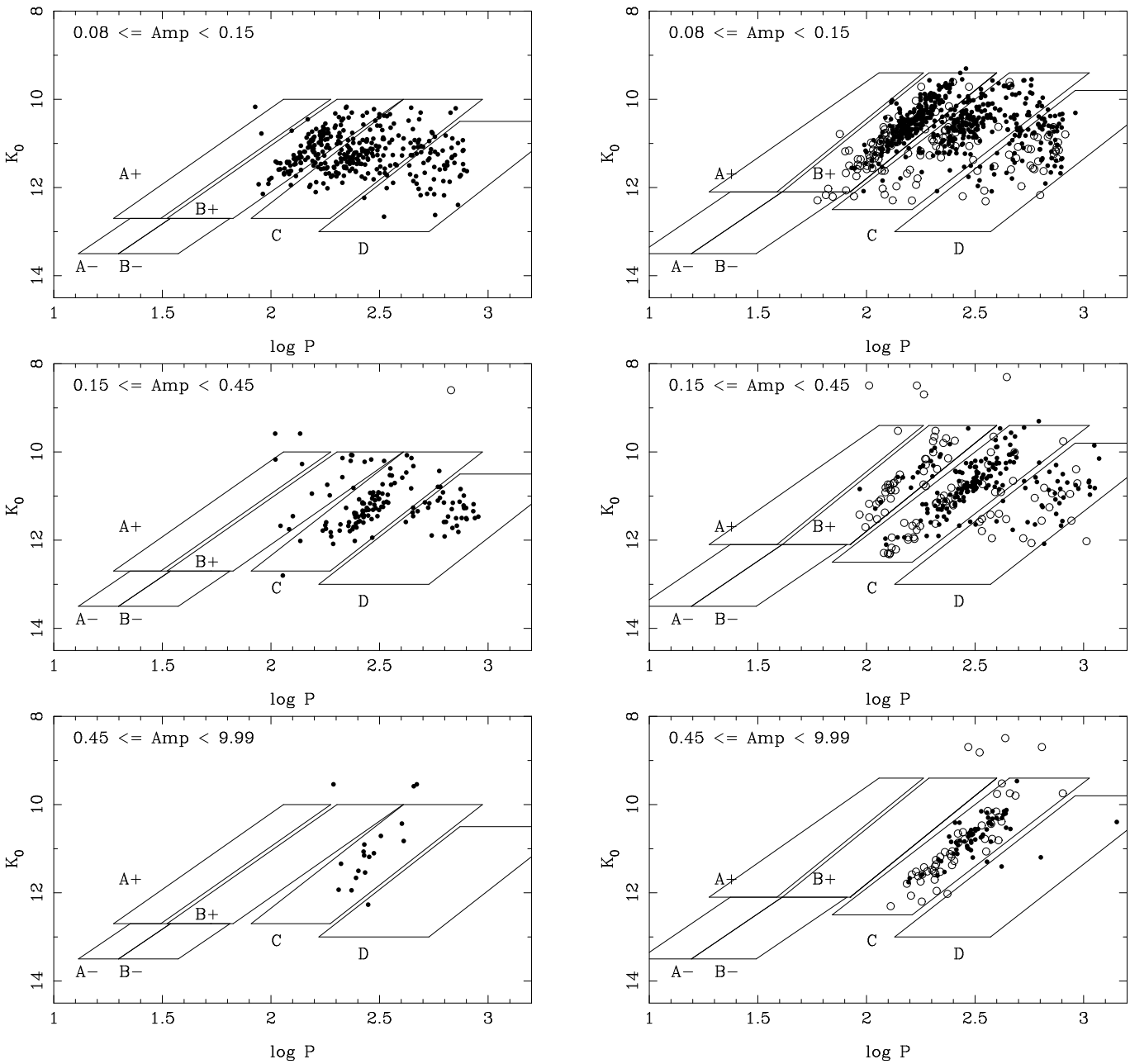

Fig. 3. Continued

4.4. Changes in periods over time

In this section possible changes in pulsation periods over time are being discussed. This is possible because the periods in the Hughes list and WBP are based on plate material typically taken between 1977 and 1984, while the MACHO, OGLE, MOA, AGAPEROS data was taken in the late-1990s, i.e. a timespan of typically 17 years. A cross-correlation of the OGLE objects was performed, but this time not with spectroscopically known objects, but rather with known LPVs with a historical period. Table 6 (complete table available in electronic form) lists the results for a total of 370 stars and is similar to Table 2. In addition the known periods are listed: first the historical period (Hughes list or WBP), then the corresponding period from OGLE, and when available other known periods (with reference between parenthesis). Since multiple periods are allowed for by the analysis of the OGLE data, the OGLE period quoted is the one for which the amplitude is similar to the one corresponding to the historical period (in some cases this then corresponds not to the primary period as determined from the OGLE data, but often to the LSP). In the last column some remarks are given concerning possible period or pulsation mode changes.

Of particular interest to look for period changes are the Miras that have defined the Mira PL-relation over the years and that have periods determined at multiple epochs (GLE81, WBP, FGWC, GLE03). In fact, GLE03 discuss 42 Miras that have defined the Mira PL-relation and in particular derive periods from the MACHO database and compare these to the historical period (FGWC, GLE81). In all but three cases they

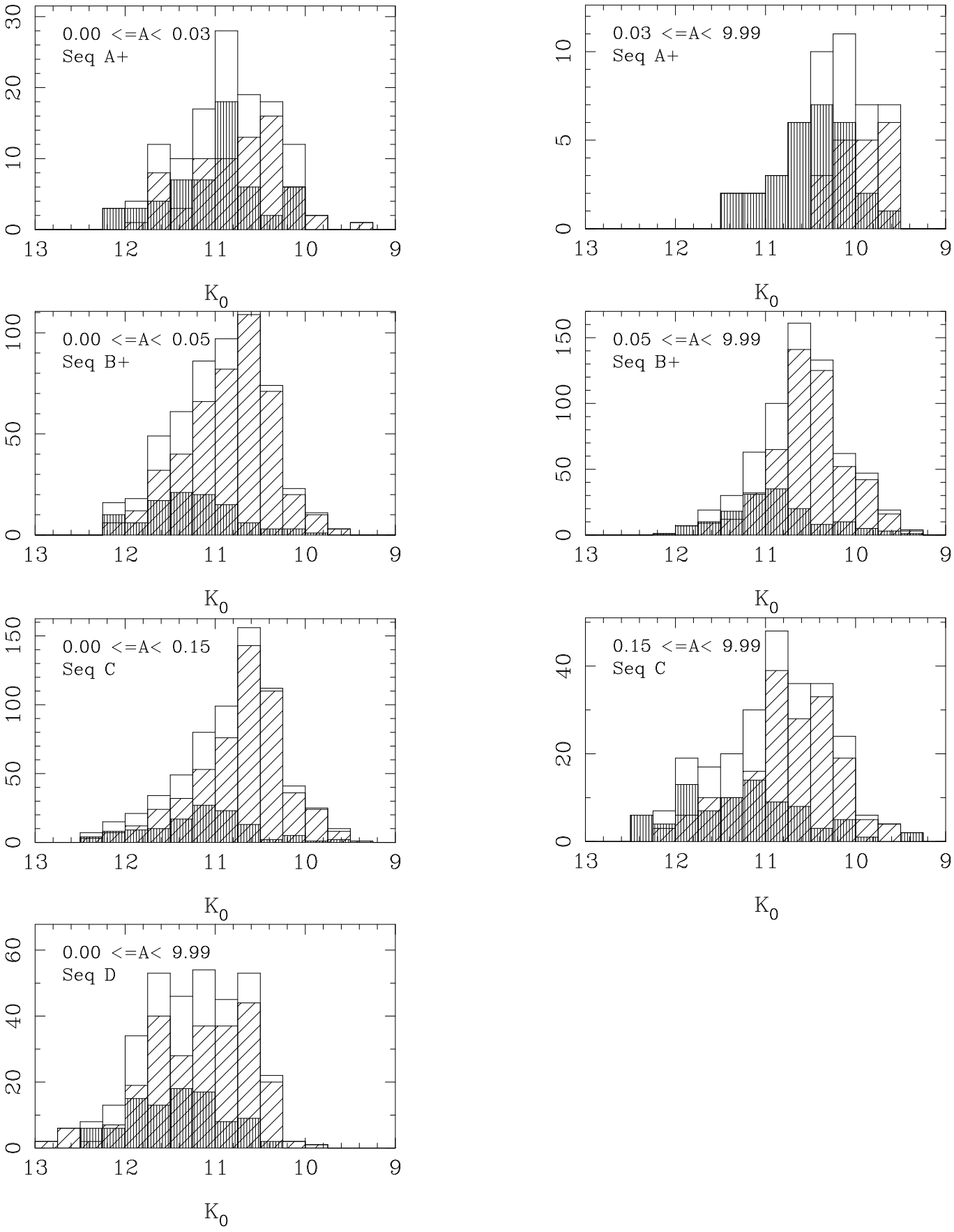

Fig. 4. Histograms of the LMC K-band 2MASS magnitude distribution for different "boxes" and I-band amplitude cuts. Shown are the histograms for the M-stars (vertical lines), C-stars (hatched), and total. The luminosity function for sequence "D" is likely to be incomplete for $K \lesssim 11$ because of the stricter conditions to accept periods above 800 days.

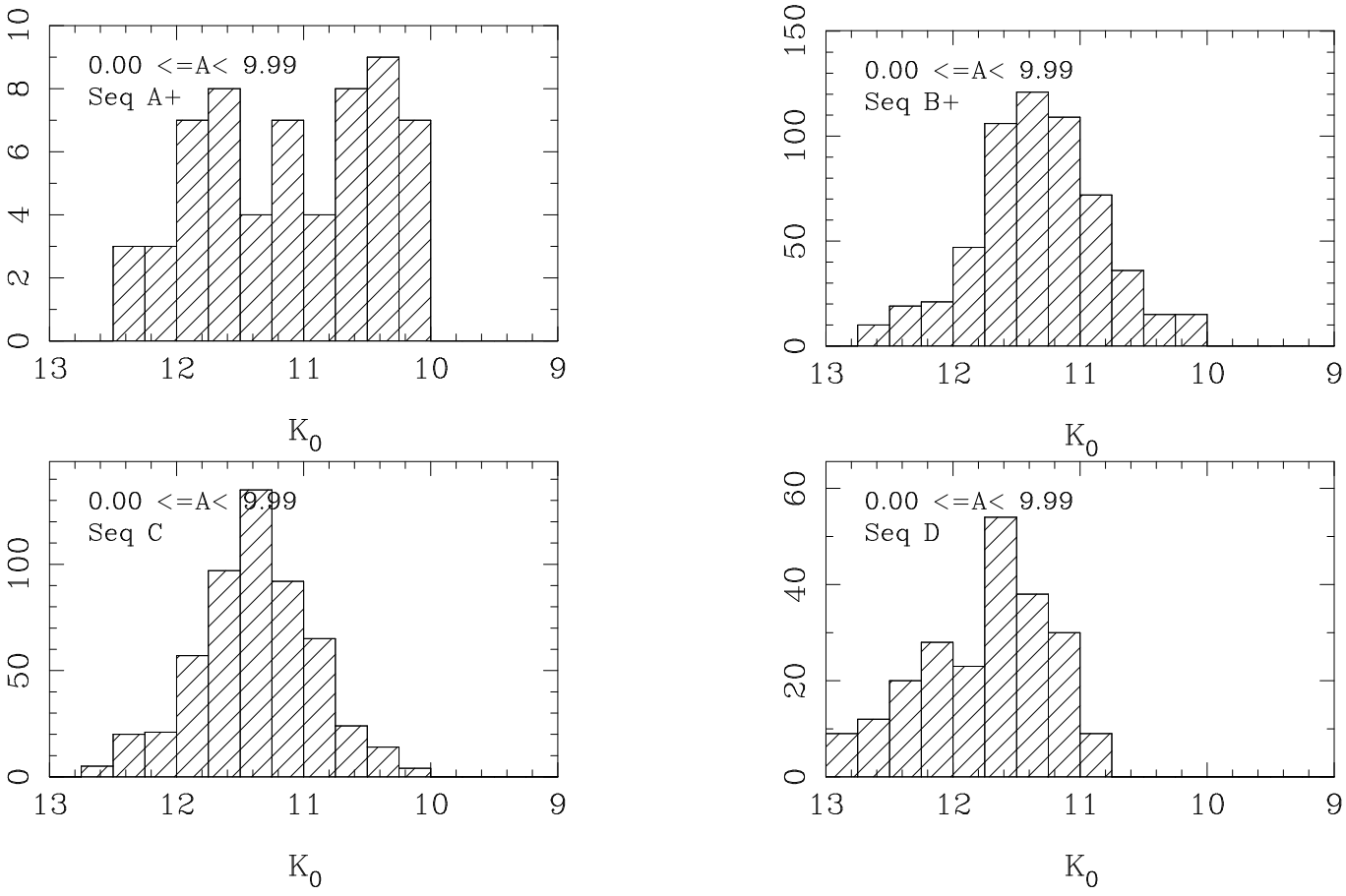

Fig. 5. As Figure 4 for the SMC.

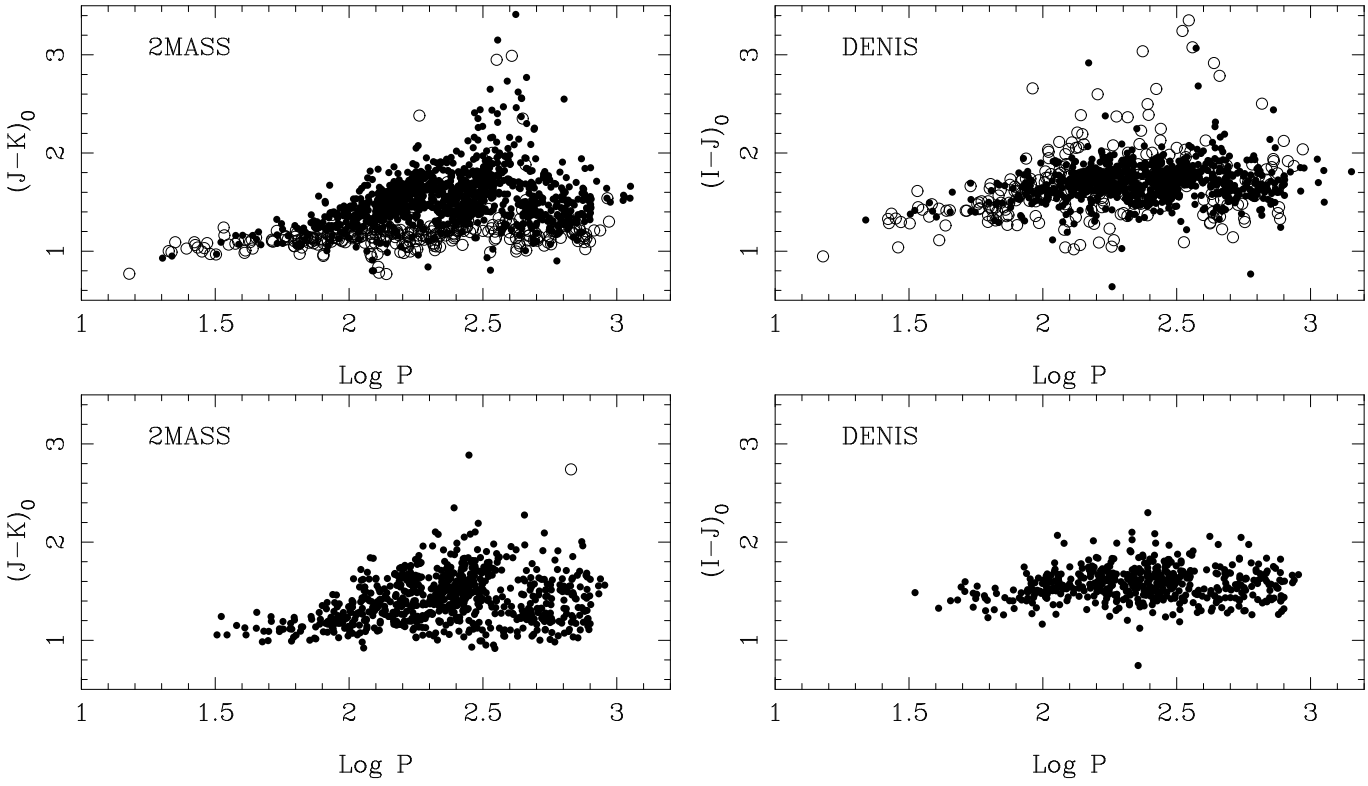

Fig. 7. Colour-Period diagram for the LMC (top left and top right) and SMC (bottom left and bottom right) objects. The period with the largest amplitude is plotted. Symbols as in Figure 3.

Table 6. First entries in the electronically available table, which list: OGLE-field, OGLE-name, other names, periods (respectively the historical period–in the majority of cases from the Hughes list or WBP–then the present-day period from OGLE and finally other available periods with reference between parentheses), spectral type and references and comments on period changes

Field	OGLE-name	Other Name	Period	SpT	Comment
lmc_sc15	OGLE050024.75-685304.8	SHV050038.5-685722	187, 376		alias, or B+ $\rightarrow$ C
lmc_sc15	OGLE050025.07-690558.0	SHV050040.7-691015	332, 344	C	
lmc_sc15	OGLE050033.74-693017.2	SHV050052.9-693434	391, 432	C	change more than 10%
lmc_sc15	OGLE050034.09-692313.2	SHV050052.2-692730	315, 310	C	
lmc_sc15	OGLE050042.90-690435.2	SHV050058.3-690851	162, 163	M6	
lmc_sc15	OGLE050045.01-691422.4	SHV050101.9-691838	317, 333	C	
lmc_sc15	OGLE050045.80-690921.8	SHV050101.9-691338	276, 283	M?	
lmc_sc15	OGLE050122.62-684324.0	SHV050135.1-684737	231, 243		
lmc_sc15	OGLE050131.98-684130.6	SHV050144.2-684542	401, 386		
lmc_sc15	OGLE050137.46-684837.8	SHV050150.7-685250	146, 146		
lmc_sc15	OGLE050141.86-692020.7	SHV050159.8-692433	386, 360	M6	
lmc_sc15	OGLE050203.62-692702.9	SHV050222.6-693113	255, 246		
lmc_sc15	OGLE050213.87-692117.6	SHV050231.9-692527	180, 177		
lmc_sc14	OGLE050228.98-692010.0	SHV050246.9-692418	310, 312	C	
lmc_sc14	OGLE050258.41-690026.9	SHV050313.7-690433	307, 302		
lmc_sc14	OGLE050303.05-691221.7	KDM_1631, SHV050319.9-691628	1003, 1169	C	peculiar, change within "D"
lmc_sc14	OGLE050328.77-692747.2	SHV050348.1-693152	464, 441	C?	
lmc_sc14	OGLE050331.05-684831.8	KDM_1683, SHV050344.6-685236	393, 381	C	
lmc_sc14	OGLE050342.24-691512.4	SHV050359.5-691915	234, 234		
lmc_sc14	OGLE050346.90-685753.8	SHV050401.8-690157	418, 375		change more than 10%
lmc_sc14	OGLE050358.30-692057.5	SHV050416.6-692500	430, 205		C $\rightarrow$ B+
lmc_sc14	OGLE050410.11-692135.2	SHV050428.6-692536	386, 395	M6	
lmc_sc14	OGLE050410.21-690743.7	SHV050426.6-691145	1353, 1475		very peculiar

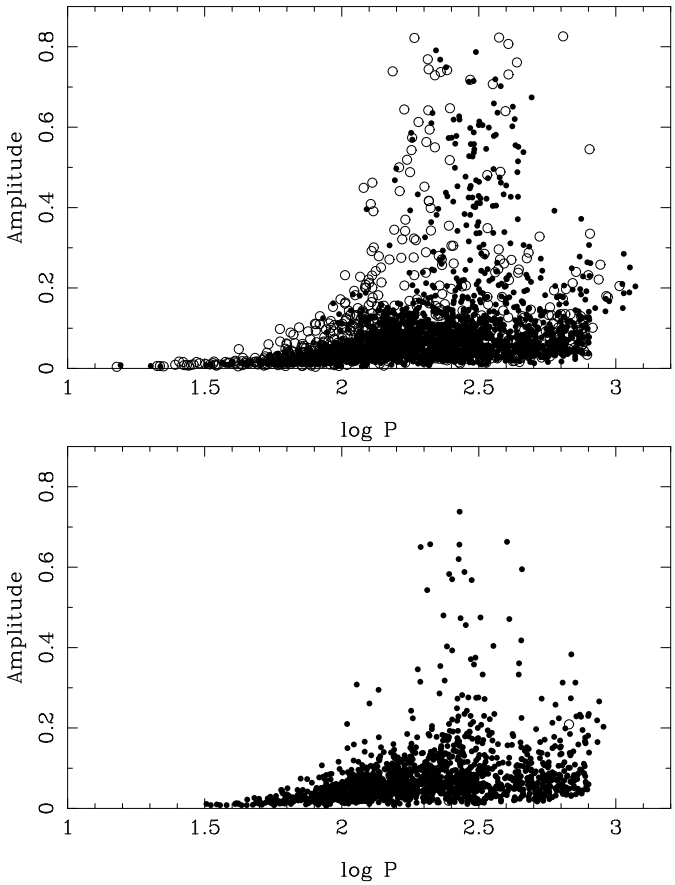

Fig. 6. Amplitudes versus periods for the LMC (left) and SMC (right) variables. Symbols as in Figure 3.

Table 5. Theoretical colours of M- and C-stars of solar metallicity. Columns 3 and 4 represent the colours for the photosphere, while, for some models, columns 5 and 6 indicate the colours when the star is obscured by circumstellar dust equivalent to a dimming in K by 0.05 mag.

SpT	$T_{\rm eff}$	$(I-J)$	$(J-K)$	$(I-J)$	$(J-K)$
M0	3850	1.18	1.08		
M3	3550	1.39	1.18	1.53	1.34
M5	3397	1.86	1.27		
M7	3129	3.11	1.37	3.73	1.97
M8	2890	3.71	1.37		
M10	2500	4.13	1.35	4.45	1.74
C	3600	1.43	1.17		
C	3400	1.56	1.30		
C	3200	1.72	1.43		
C	2800	2.00	1.61		
C	2650	2.09	1.61	2.48	2.09

found the periods to be constant over 2 to 3 decades. The three are WBP-30 which changed from a 400d Mira into a small amplitude variable with 183d period, GR0537-6740 whose period changed from 418 to 367d, and GR17 whose period changed from 780 to 729d. In the other objects the change in period was less than 3% of the period.

Figure 8 shows that K-band PL-relation for the stars that changed the period by more then 0.1 dex, and with historical and recent period connected by a thin line. Several objects seem to have changed period considerably and changed pulsation mode. The data on these stars have been carefully checked in terms of positional association, period determination, amplitude, I and JK magnitudes when available, etc. These stars

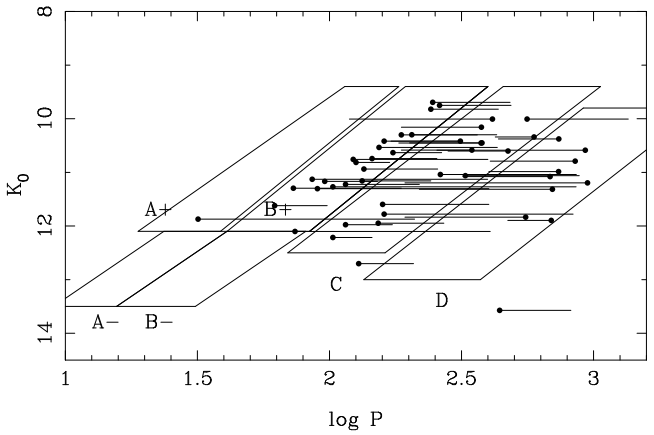

Fig. 8. K-band PL-relation for the (LMC) stars that have undergone a period change over the past two decades of at least 0.1 dex. Historical and current period are connected by a line, with the current period marked by a solid circle.

have been marked in Table 6, as well as other stars that changed period by more than 10% (30 objects). These smaller changes may very well be real but in most cases too small to be related to a change in pulsation mode. Most of the changes occur from box "C" to "B+" (15 out of 36), and from "C" to "D" (8/36). Unfortunately, the original data points of the stars from the Hughes list are not available to directly phase the old data points with the present day period to verify the change in period. Figure 9 shows some of the lightcurves of the stars that possibly changed pulsation mode (complete figure available in the electronic edition). As is evident many of them are far from being regular.

Possibly the best studied case of mode switching in a Galactic Mira-like variable is that of R Dor. Bedding et al. (1998) show that the star switches back and forth between two pulsation period of 332 and about 175 days, on a time scale of about 1000 days. The star has an accurate (Hipparcos) parallax and hence can be placed in Figure 8. For any reasonable distance to the LMC it implies the star moves back and forth between sequences "C" and "B+".

Figure 10 shows the distribution of the ratio (current period / historical period) near a value of 1. The observed mean is 1.00018. Also a Gaussian fit to this distribution is shown to guide the eye, which has a dispersion of 0.031. As stars evolve to cooler temperature and lower mass on the AGB one might expect an increase of the pulsation period. To verify this theoretically, the synthetic AGB evolution code based on the formulation in Wagenhuber & Groenewegen (1998) was used for a typical star with 2 $M_\odot$ initial mass and metallicity Z = 0.008. The model takes into account the changes in stellar parameters over the thermal pulse cycles, and assumes that pulsation takes place over the entire TP-AGB, i.e. no cessation of pulsation or mode switches during any phase of the stars' TP-AGB evolution. For every time step the fundamental and first overtone pulsation period was calculated from $P_0 = 0.00851 R^{1.94} M^{-0.90}$ and $P_1 = 0.038 R^{1.5} M^{-0.5}$ (Wood 1990; R being the stellar radius in solar radii, and M the total mass in solar masses). Figure 11 shows the distribution function of P_0 and P_1 over a timespan of 17 years for such an object, both on a linear and logarithmic scale. The AGB evolution is such that on average a star evolves to longer period with time, but almost not measurably so over 17 years. Indeed the averages are 1.00024 for fundamental mode and 1.00015 for first overtone. This implies that for any individual star one must be able to determine periods to fractions of a day to be able to detect period changes due to evolution, which seems unrealistic since the lightcurves are rather complicated and not mono-periodic in the majority of cases. The fact that the observed mean of the period ratios over a 17 year timespan is close to the predicted one probably indicates good fortune rather than to indicate that, in a statistical sense, the predicted evolutionary effect has indeed been detected. The width of the observed distribution is much wider than predicted by the models, and is also wider than expected from the errors in the observed period determinations alone. The median period of the stars listed in Table 6 is about 290 days, and in the overall majority of cases such a period has been determined with an accuracy of 0.7 days, or better. This implies one would expect ratios near unity with an error of about 0.005 or smaller. This would suggest that the width of the distribution is real.

In addition, there exist a few examples of LPVs whose period *decrease* over a longer timescale (Wood & Zarro 1981). Zijlstra et al. (2002) show that for the Mira R Hya $\dot{P}$ is about $-1.6\ 10^{-3}$ between 1770 and 1950 AD. Although its period has actually stabilised at 385d since then, let us assume it would follow its historical trend. Over a 17 year period it would decrease its period by 9.9 days and would have a period ratio, as defined and used in Figures 10 and 11, of 0.975. These values are predicted by the stellar evolutionary calculations mentioned above (and by the calculations in Wood & Zarro) but with a very small probability. The fact that the observed distribution in Figure 10 is wider than expected, based on the errors alone, suggests that other phenomena than the "global" increase in period over an AGB stars lifetime dominate this distribution, or that a model assumption is incorrect. Either pulsation does not take place at all phases of AGB evolution which would influence the theoretically predicted distribution function, or other physical phenomena play a role. Zijlstra et al. (2002) mention and refer to weak chaotic behaviour and the effects of the non-linearity of the pulsation in the case of R Hya.

4.5. Very red objects

Since the spectroscopically selected sample, for given luminosity, will be biased against stars with heavy mass loss, and hence fainter I magnitudes, the present section discusses an infrared selected sample with red infrared colours, which will complement the sample of spectroscopically selected AGB stars. Figure 12 shows the DENIS $K_0 - (I-K)_0$ magnitude-colour, $(I-J)_0 - (J-K)_0$ colour-colour, and the 2MASS $K_0 - (J-K)_0$ magnitude-colour, $(J-H)_0 - (H-K)_0$ colour-colour diagrams for both LMC and SMC for the spectroscopically selected sample in the two leftmost columns. Based on this diagram it was decided to investigate the pulsation characteristics of objects that have DENIS $(I-K)_0 > 4.0$ and

Fig. 9. Representative lightcurves of stars that have changed pulsation mode over the last 2 decades. The fit is indicated by the (red) solid line. Crosses indicate data points not included in the fit. Complete figure is available in the electronic form.

$(\sigma_{\rm I}^2+\sigma_{\rm K}^2)/(I-K)_0 < 0.01$ or 2MASS $(J-K)_0 > 2.0$ and $(\sigma_{\rm J}^2+\sigma_{\rm K}^2)/(J-K)_0 < 0.01$.

The infrared selected sample contains 577 objects (137 SMC, 442 LMC) that fullfill these limits and Figure 13 shows the lightcurves of the reddest stars in $(J-K)$ among them (the full figure is available in the electronic edition). Tables 7 and 8 show the first entries with information similar to Tables 2 and 3. The colour-colour diagrams are shown in the two right side columns in Figure 12. Some stars from the spectroscopically selected sample also appear in the infrared selected sample, mostly M-stars for which it is was shown before that the later spectral types are reasonably red in $(I-K)$, certainly compared to carbon stars for a given $(J-K)$.

Figure 14 finally shows the K-band PL-relation for the large amplitude variables in the infrared selected sample. Compared to stars that are spectroscopically known they appear to be fainter at a given period. This must be largely due to the dust obscuration. An identical effect was shown by Wood (2003) who specifically looked at MSX sources. To illustrate this, Figure 15 shows the spectral energy distribution of one of the stars in Figure 14, namely OGLE050854.21-690046.4 or MSX 83. For a distance of 50.1 kpc, a luminosity of 22100 $L_\odot$ is derived and a mass loss rate of 7.6 $\times 10^{-6}$ $M_\odot$ yr^{-1}.

5. Summary and discussion

This paper addresses several aspects of the pulsational character of late-type stars in the Magellanic Clouds. The main focus is on the K-band PL-relation of almost 2300 spectroscopically confirmed M-,S- and C-stars. This sample avoids to make the

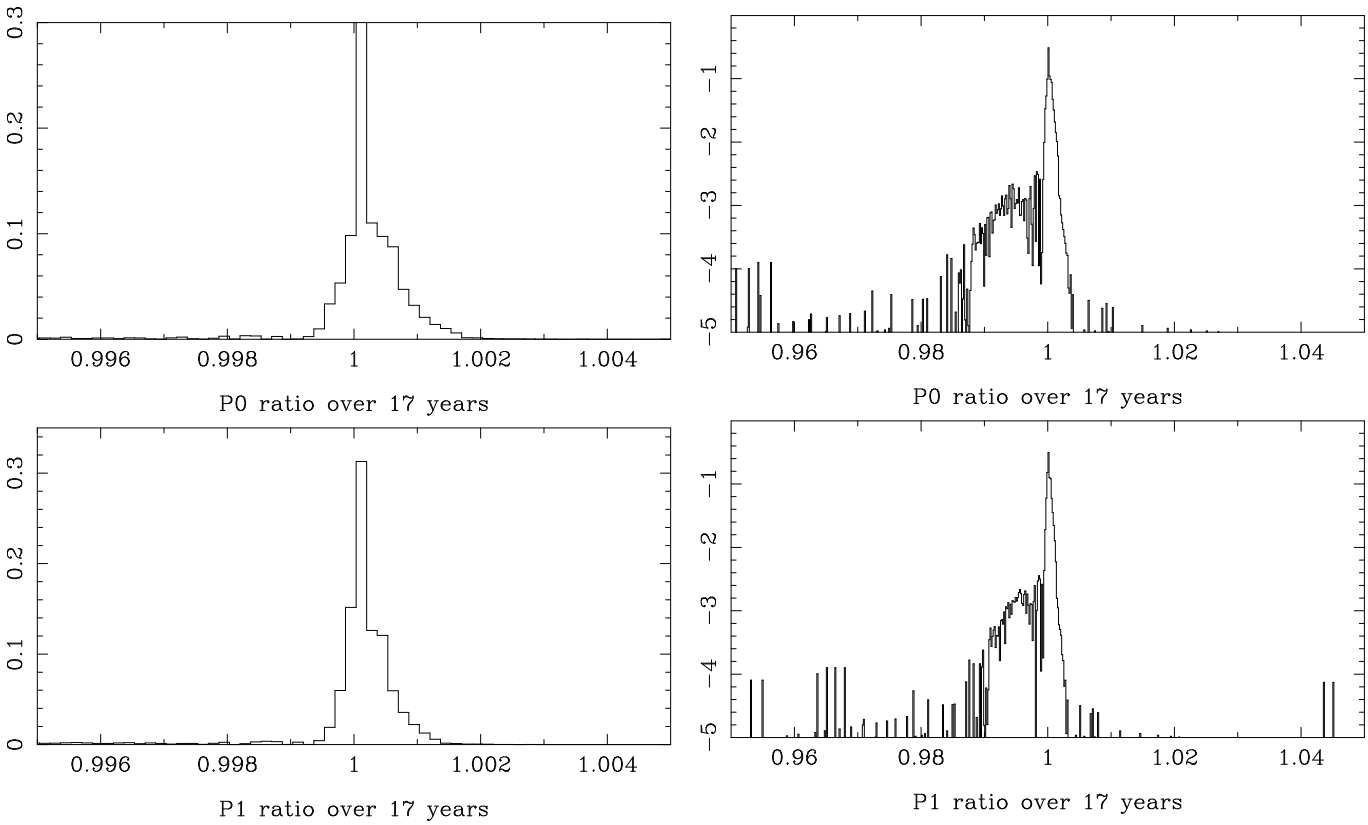

Fig. 11. Distribution function of the ratio of the fundamental (top panels) and first overtone (bottom panels) pulsation period over a 17 year timespan, on a linear (left-hand side), and logarithmic (right-hand side) scale for a 2 $M_\odot$ star with typical LMC metallicity. The AGB evolution is such that on average a star evolves to longer periods with time, but not measurably so over 17 years.

Table 7. The infrared selected sample. As Table 2.

Field	OGLE-name	Period	Amp	Period	Amp	Period	Amp	$I_{\rm ogle}$	$I_{\rm denis}$	$J_{\rm denis}$	$K_{\rm denis}$	$J_{\rm 2MASS}$	$H_{\rm 2MASS}$	$K_{\rm 2MASS}$
smc_sc1	OGLE003633.20-735432.5	0.0 ± 0.000	0.000	0.0 ± 0.000	0.000	0.0 ± 0.000	0.000	16.61	16.11 ± 0.03	13.90 ± 0.03	11.00 ± 0.02	14.14 ± 0.03	12.55 ± 0.03	11.25 ± 0.03
smc_sc1	OGLE003720.78-730944.4	128.3 ± 0.316	0.117	424.9 ± 0.680	0.734	0.0 ± 0.000	0.000	19.04	99.00 ± 9.99	99.00 ± 9.99	99.00 ± 9.99	16.04 ± 0.11	13.63 ± 0.03	11.85 ± 0.02
smc_sc1	OGLE003732.32-733021.3	213.6 ± 3.556	0.025	1192.8 ± 99.000	0.597	2056.4 ± 99.000	0.736	18.44	99.00 ± 9.99	99.00 ± 9.99	99.00 ± 9.99	16.08 ± 0.09	14.62 ± 0.05	13.60 ± 0.05
smc_sc1	OGLE003801.87-734725.7	315.0 ± 0.508	0.142	494.8 ± 0.189	0.640	0.0 ± 0.000	0.000	15.58	16.19 ± 0.05	13.79 ± 0.03	99.00 ± 9.99	13.81 ± 0.02	12.23 ± 0.02	10.79 ± 0.02
smc_sc1	OGLE003830.92-733113.6	100.0 ± 0.026	0.243	158.7 ± 0.052	0.380	384.2 ± 1.362	0.079	15.31	14.74 ± 0.02	13.00 ± 0.01	10.54 ± 0.01	13.08 ± 0.02	11.68 ± 0.03	10.72 ± 0.02
smc_sc1	OGLE003848.77-735601.1	280.2 ± 0.153	0.588	640.1 ± 9.035	0.179	1499.2 ± 16.100	1.448	17.22	16.76 ± 0.05	15.18 ± 0.17	12.17 ± 0.04	15.20 ± 0.07	13.56 ± 0.05	12.28 ± 0.03
smc_sc2	OGLE004010.23-730039.4	188.2 ± 0.195	0.128	351.5 ± 0.151	0.774	1979.9 ± 24.789	0.510	15.75	15.78 ± 0.05	13.68 ± 0.04	10.90 ± 0.03	14.43 ± 0.03	12.80 ± 0.03	11.45 ± 0.02
smc_sc2	OGLE004014.23-724959.2	236.1 ± 1.436	0.206	250.3 ± 1.534	0.219	1095.9 ± 3.420	0.203	14.51	14.80 ± 0.02	12.66 ± 0.02	10.52 ± 0.02	12.58 ± 0.03	11.30 ± 0.02	10.51 ± 0.02
smc_sc2	OGLE004016.25-730115.1	157.5 ± 0.755	0.054	480.5 ± 0.925	0.853	1503.1 ± 19.637	0.648	18.10	17.00 ± 0.11	15.87 ± 0.25	12.26 ± 0.10	14.28 ± 0.04	12.46 ± 0.03	10.97 ± 0.02
smc_sc2	OGLE004027.57-732611.0	141.4 ± 0.126	0.086	269.5 ± 0.135	0.481	515.5 ± 1.259	0.176	15.76	15.86 ± 0.04	14.08 ± 0.04	11.74 ± 0.06	13.38 ± 0.03	12.23 ± 0.02	11.28 ± 0.02
smc_sc2	OGLE004032.93-732839.7	551.2 ± 0.643	1.263	0.0 ± 0.000	0.000	0.0 ± 0.000	0.000	18.66	17.30 ± 0.19	14.20 ± 0.07	10.79 ± 0.03	15.61 ± 0.08	13.39 ± 0.04	11.57 ± 0.03
smc_sc2	OGLE004035.31-731928.7	508.7 ± 0.765	0.881	0.0 ± 0.000	0.000	0.0 ± 0.000	0.000	18.85	99.00 ± 9.99	99.00 ± 9.99	99.00 ± 9.99	16.28 ± 0.12	14.18 ± 0.05	12.30 ± 0.03
smc_sc2	OGLE004114.43-731008.8	625.2 ± 3.056	0.943	862.6 ± 30.639	0.352	0.0 ± 0.000	0.000	18.74	99.00 ± 9.99	99.00 ± 9.99	99.00 ± 9.99	16.26 ± 0.11	13.97 ± 0.05	11.97 ± 0.03
smc_sc2	OGLE004116.95-725216.4	384.3 ± 0.446	0.629	1484.6 ± 16.917	0.688	548.0 ± 8.036	0.121	15.92	16.18 ± 0.05	13.85 ± 0.04	11.19 ± 0.03	14.00 ± 0.03	12.33 ± 0.03	10.98 ± 0.02
smc_sc2	OGLE004142.44-725853.2	415.8 ± 0.343	0.336	0.0 ± 0.000	0.000	0.0 ± 0.000	0.000	15.85	16.42 ± 0.07	13.52 ± 0.03	11.75 ± 0.05	13.67 ± 0.02	12.00 ± 0.03	10.64 ± 0.02
smc_sc2	OGLE004152.05-730827.4	366.7 ± 0.185	0.580	1538.7 ± 6.836	0.726	0.0 ± 0.000	0.000	16.69	99.00 ± 9.99	99.00 ± 9.99	99.00 ± 9.99	13.90 ± 0.02	12.27 ± 0.03	11.05 ± 0.05
smc_sc2	OGLE004156.80-730728.9	241.5 ± 0.218	0.125	475.4 ± 0.248	0.331	935.1 ± 3.473	0.168	14.21	14.09 ± 0.01	12.13 ± 0.01	10.10 ± 0.01	12.28 ± 0.02	11.01 ± 0.02	10.16 ± 0.02
smc_sc2	OGLE004217.65-733419.1	131.9 ± 0.026	0.489	0.0 ± 0.000	0.000	0.0 ± 0.000	0.000	15.61	15.04 ± 0.01	13.24 ± 0.01	10.78 ± 0.01	13.60 ± 0.03	12.19 ± 0.03	11.02 ± 0.02
smc_sc3	OGLE004235.80-730920.9	121.6 ± 0.159	0.066	493.7 ± 0.244	0.899	1959.7 ± 27.705	0.416	17.44	17.49 ± 0.18	14.66 ± 0.09	11.28 ± 0.04	15.30 ± 0.05	13.29 ± 0.02	11.73 ± 0.03
smc_sc3	OGLE004240.89-725705.1	221.6 ± 0.295	0.173	491.8 ± 0.870	0.681	1395.1 ± 6.272	0.861	17.24	16.53 ± 0.08	15.24 ± 0.11	11.40 ± 0.03	13.22 ± 0.03	11.61 ± 0.03	10.16 ± 0.02
smc_sc3	OGLE004243.06-731841.7	382.1 ± 0.126	0.790	1127.0 ± 4.118	0.245	0.0 ± 0.000	0.000	17.04	99.00 ± 9.99	99.00 ± 9.99	99.00 ± 9.99	13.62 ± 0.05	12.23 ± 0.05	11.08 ± 0.03
smc_sc3	OGLE004253.55-725622.2	359.3 ± 1.282	0.539	1845.9 ± 99.000	0.431	0.0 ± 0.000	0.000	15.89	15.76 ± 0.04	13.61 ± 0.03	10.97 ± 0.02	13.13 ± 0.02	11.77 ± 0.02	10.78 ± 0.03
smc_sc3	OGLE004309.55-730922.2	383.6 ± 0.215	0.873	0.0 ± 0.000	0.000	0.0 ± 0.000	0.000	18.43	99.00 ± 9.99	99.00 ± 9.99	99.00 ± 9.99	14.18 ± 0.07	12.28 ± 0.05	10.79 ± 0.04

clearly incorrect approximation made in other studies that M-stars and carbon stars can be separated at a colour $(J-K)$ = 1.4.

The present observations however do not allow the presentation a comprehensive picture of the evolution of pulsation periods of M- and C-stars. This would require a more detailed (AGB star) population synthesis study including pulsation properties. As previous MCs studies have found for AGB stars in general (Wood et al. (1999), Wood (2000), Noda et al. (2002), Lebzelter et al. (2002), Cioni et al. (2003), Ita et al. (2004a,b) and Kiss & Bedding (2003, 2004)), it is found specifically that both M-, and C-stars tend to occupy preferentially sequences B+ and then C for increasing amplitude. For a given amplitude, the C-stars tend to have the longer period, and, for a every sequence they are more luminous. This effect has previously been observed in MC clusters (e.g. FMB) and is in qualitative agreement with evolutionary calculations that predict that C-stars evolve from M-stars.

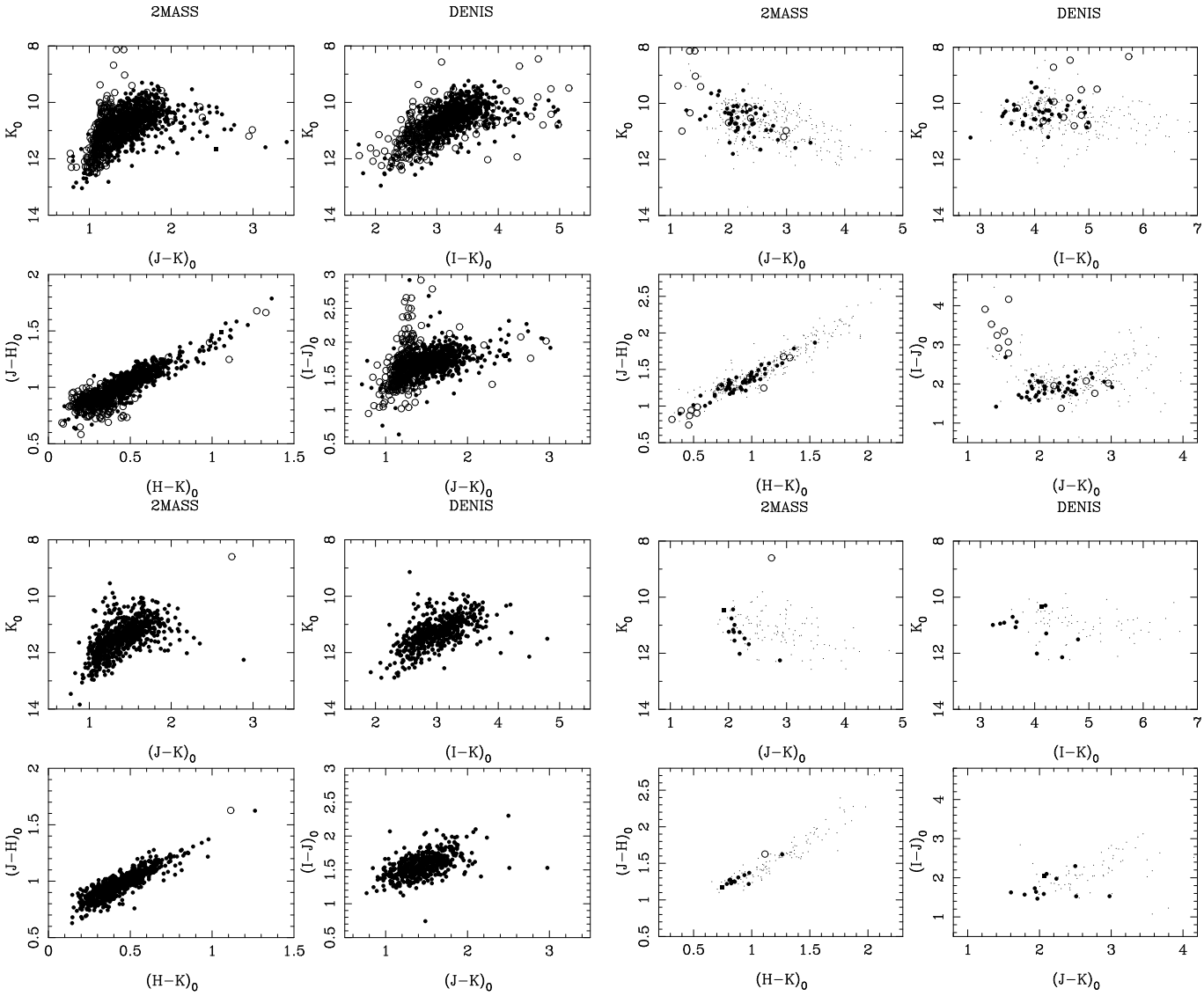

Fig. 12. LMC (top 2 rows) and SMC (bottom 2 rows) colour-colour diagrams using 2MASS and DENIS photometry for the spectroscopically selected sample (left 2 columns) and the infrared selected sample (right 2 columns). Note the difference in scale! Symbols as in Figure 3, with dots indicating objects without spectroscopic classification.

Many objects have one period that falls in box "D". In the spectroscopically selected sample, 211 of 859 SMC stars (= 24.6%) have a period that falls in box "D", and 318 of the 1418 LMC stars (= 22.4%, namely 229/1064 = 21.5% of C-stars and 89/354 = 25.1% of M-stars). As will be discussed below, for at least some stars of the IR selected sample this is due to the fact that they are weaker in K because of dust obscuration. For the overall majority of the stars in the spectroscopically selected sample this is not an issue. The reason why some late-type stars appear on that location of the PL-diagram is unexplained, see the discussion in Olivier & Wood (2003), Wood (2003, 2004). The classical large-amplitude Mira variables appear on sequence "C" (see the last panels in Figure 3) and are believed to be fundamental-mode pulsators, hence longer (radial mode pulsation) periods should not exist. The present paper does not shed light into the nature of the LSP phenomenon, except that Figure 4 indicates that the K-band luminosity function for sequence "D" is essentially the same for the M- and C-stars, while for sequences "A,B,C" the C-stars are brighter, as expected from an evolutionary point of view. The luminosity function of objects on sequence "D" is fainter from those of the other sequences. This is due to the fact that periods longer than 800 days are underrepresented because of stricter selection rules. This affects predominatly sequence "D" objects with K_0 $\lesssim$10.5 mag. The fact that the fraction of all object with periods on sequence "D" is essentially the same for C- and M-stars and that the K-band luminosity of C- and M-stars of sequence "D" objects is very similar suggests that the LSP phenomenon is unrelated to chemical type, and hence seems unrelated to a pulsation phenomenon.

For a few hundred variables it was possible to look for period changes over a timespan of typically 17 years. Almost all come from the studies by Hughes (1989) and Hughes & Wood (1990). They identified medium to large amplitude variables

fig13.jpg

Fig. 13. Lightcurves of the reddest stars in $(J-K)$. Note the faintness in I. Nine of the 15 stars have been detected in the MSX survey. Complete figure is available in electronic form.

from photographic material using typically 21 observations in the time span 1977 to 1984. Out of 370 objects, 36 have been identified that seemingly changed pulsation mode (or at least changed "box") between $\sim$1980 and the time of the OGLE observations, and another 30 objects that changed pulsation period by more than 10%. This ratio of about 10% (36/370) is similar to the study of GLE03 who found large period changes in 3 out of 42 Mira variables studied. A caveat is that the original historical data points have never been published, and it would certainly be preferable to be able to phase the old data with the current period to see if in fact the period change is real. For the moment I consider the 10% change of pulsation sequence over $\sim$17 years as an upper limit. By comparison, Zijlstra & Bedding (2003) find that only of order of 1% of well-known Miras show evidence for period changes. The understanding for MC objects may improve because of ongoing (e.g. OGLE-III) and future surveys.

Finally a sample of stars was studied selected on infrared colours, namely redder than the majority of the spectroscopically selected sample. It should be pointed out that there is no proof that these are AGB stars (except for the few ones in overlap with the spectroscopically selected sample) and they make suitable targets for spectroscopic follow-up to determine their spectral type. Many of these stars also have a period located in box "D" but in this case the effect of obscuration by dust must be considered. This also has implications when using samples of variables to determine K-band PL-relations. In the last section one explicit example was shown, namely MSX 83, for which the SED was constructed and fitted with a dust radiative transfer model. Its period of 611 day, and K magnitude of 10.58 would put it in "box D". However, when running the radiative transfer model without mass-loss the K-magnitude brightens to 9.17 mag (this value is somewhat dependent on the central star model atmosphere assumed) putting it on the

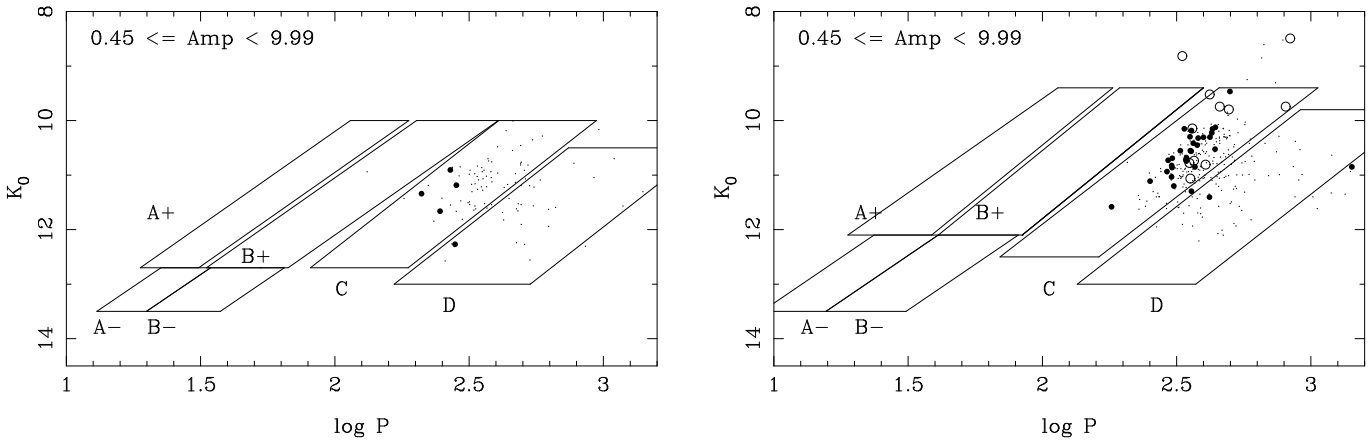

Fig. 14. K-band PL-relation for the large amplitude variables in the IR selected sample, for the SMC (left) and LMC (right).

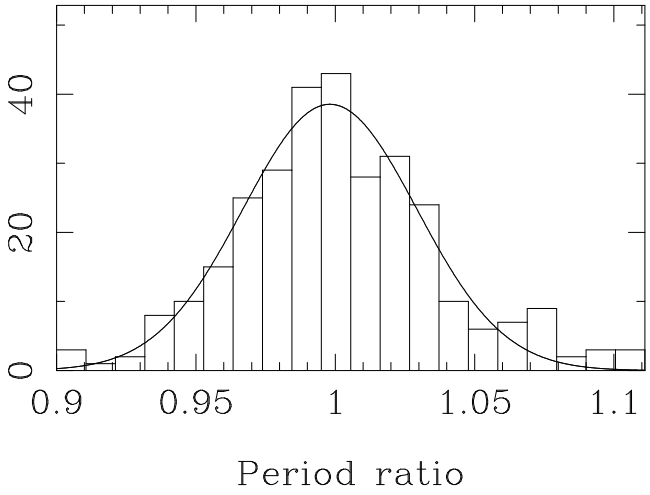

Fig. 10. Distribution function of the ratio of the historical to the current period near a value of unity. The mean of all values is 1.00179. The solid line is a Gaussian fit with a σ of 0.031, centered at 0.9981.

Table 8. The infrared selected sample. As Table 3.

Field	OGLE-name	Other Name	SpT	Comments
smc_sc1	OGLE003633.20-735432.5			
smc_sc1	OGLE003720.78-730944.4			
smc_sc1	OGLE003732.32-733021.3			
smc_sc1	OGLE003801.87-734725.7			
smc_sc1	OGLE003830.92-733113.6			
smc_sc1	OGLE003848.77-735601.1	MH_0400	C	
smc_sc2	OGLE004010.23-730039.4			
smc_sc2	OGLE004014.23-724959.2			
smc_sc2	OGLE004016.25-730115.1			
smc_sc2	OGLE004027.57-732611.0			
smc_sc2	OGLE004032.93-732839.7			
smc_sc2	OGLE004035.31-731928.7			
smc_sc2	OGLE004114.43-731008.8	[WSH2003] a- 8		
smc_sc2	OGLE004116.95-725216.4			
smc_sc2	OGLE004142.44-725853.2			
smc_sc2	OGLE004152.05-730827.4			
smc_sc2	OGLE004156.80-730728.9			
smc_sc2	OGLE004217.65-733419.1			
smc_sc3	OGLE004235.80-730920.9			
smc_sc3	OGLE004240.89-725705.1			
smc_sc3	OGLE004243.06-731841.7			
smc_sc3	OGLE004253.55-725622.2			
smc_sc3	OGLE004309.55-730922.2			

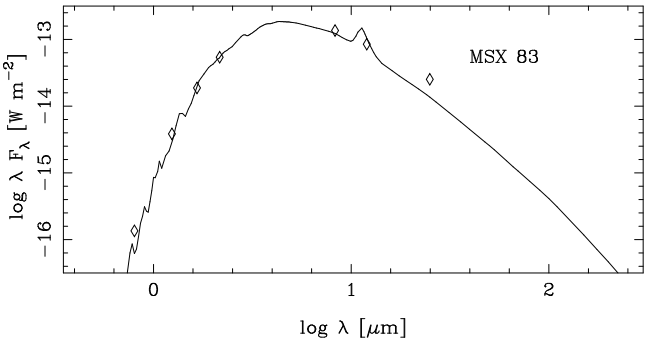

Fig. 15. SED of one of the stars in the IR selected sample, MSX 83 annex OGLE050854.21-690046.4. Plotted are the OGLE I, 2MASS JHK, MSX A band and IRAS 12 and 25 μm fluxes. A carbon star central star model is assumed.

extension of box "C", consistent with the expected location for a star with an pulsation amplitude of 0.66 mag.

In reverse this implies that when studying the K-band PL-relation, and when multi-colour data is available, a cut-off in colour should be applied in order to avoid a bias by including stars that are dust obscured in K. Although this seems obvious, a quantification of where this cut-off should be placed and its actual application are rare in the literature; In fact I could only find one instance. Glass et al. (1995) mention they exclude some faint outliers with $(K-L) \sim 2$ in the Sgr I bulge field (which corresponds to roughly $(J-K) \sim 3.5$, Glass, 1986), but did not impose a colour criterium a-priori. In other papers where dust obscuration in the studied variables should play a role the bolometric PL-relation is studied (e.g. WFLZ), which circumvents this problem in a natural way.

It is difficult to give an exact colour cut-off to apply, since this depends on the colours involved, the dust properties and the evolution of mass-loss on the AGB. Based on the calculations presented in the last columns in Table 5 stars with colours $(J-K)_0 > 2.0$ should certainly be avoided, and a stricter criterium would be to include M-stars only when $(J-K)_0 < 1.4$ and C-stars only when $(J-K)_0 < 1.7$.

Finally, applying these latter cut-offs to the spectroscopically selected stars in box "C" with amplitudes > 0.45 mag and > 0.15 mag, to improve the statistics, the K-band PL-

relations listed in Table 9 have been derived, where also some relations from the literature are listed. The period distribution of these samples is shown in Figure 16. It would be interesting to fit the SEDs of all infrared selected stars to be able to include the dust-correced K-magnitudes in these PL-relations.

There is very good agreement between the new relations (including what appears to be the first Mira K-band PL-relation in the SMC) and previous works. The formal error on the zero point and slope have become smaller, because of the larger sample size, but the overall rms are still larger because the photometry used in FGWC and GLE03 are averages over the lightcurve while the present data are at best averages of two measurements.

Acknowledgements. The author would like to thank Laurent Eyer for interesting discussions, Peter Wood (MSSSO), Mathias Schultheis (IAP) and Maria-Rosa Cioni (ESO) for providing computer readable versions of relevant data, Yoshifusa Ita for providing the boundaries of the sequences in the K-band PL-diagram in Ita et al. (2004a), Joris Blommaert for commenting on an earlier draft, and an anonymous referee for a very carefull reading of the manuscript.

This research has made use of the SIMBAD database, operated at CDS, Strasbourg, France.

This publication makes use of data products from the Two Micron All Sky Survey, which is a joint project of the University of Massachusetts and the Infrared Processing and Analysis Center/California Institute of Technology, funded by the National Aeronautics and Space Administration and the National Science Foundation.

This paper utilizes public domain data originally obtained by the MACHO Project, whose work was performed under the joint auspices of the U.S. Department of Energy, National Security Administration by the University of California, Lawrence Livermore National Laboratory under contract No. W-7405-Eng-48, the National Science Foundation through the Center for Particle Astrophysics of the University of California under cooperative agreement AST-8809616, and the Mount Stromlo and Siding Spring Observatory, part of the Australian National University

References

Alard C., Blommaert J.A.D.L., Cesarsky C., et al., 2001, ApJ 552, 289
Alcock C., Allsman R.A., Alves D.R., et al., 1997, AJ 114, 326
Alcock C., Allsman R.A., Alves D.R., et al., 1998, AJ 115, 1921
Alcock C., Allsman R.A., Alves D.R., et al., 1999, ApJ 511, 185
Alcock C., Allsman R.A., Alves D.R., et al., 2000, ApJ 542, 257
Alcock C., Allsman R.A., Alves D.R., et al., 2001, ApJ 554, 298
Afonso C., Albert J.N., Alard C., et al., 2003, preprint
Bayne G., Tobin W., Pritchard J.D., et al., 2002, MNRAS, 331, 609
Bedding T.R., Zijlstra A.A., Jones A., Foster G., 1998, MNRAS 301, 1073
Bessell M.S., Wood P.R., Lloyd Evans T., 1983, MNRAS 202, 59 (BWL)
Blanco V.M., McCarthy M.F., Blanco B.M., 1980, ApJ 242, 938 (BMB)
Blanco V.M., McCarthy M.F., 1990, AJ 100, 674 (BM)
Blanco V.M., Richer H.B., 1979, PASP 91, 659
Castilho B.V., Gregorio-Hetem J., Spite F., Spite M., Barbuy B., 1998, A&AS 127, 139
Cioni M.-R.L., Blommaert J.A.D.L., Groenewegen M.A.T., et al., 2003, A&A 406, 51 (CBG03)
Cioni M.-R.L., Loup C., Habing H.J., et al., 2000, A&AS 144, 235 (DCMC)
Cioni M.-R.L., Marquette J.-B., Loup C., et al., 2001, A&A 377, 945 (CML)
Cutri R.M., Skrutskie M.F., Van Dyk S., et al., 2003, Explanatory Supplement to the 2MASS All-Sky Data Release
Delmotte N., Loup C., Egret D., Cioni M.-R., Pierfederici F, 2002, A&A 396, 143
Demers S., Irwin M.J., Kunkel W.E., 1993, MNRAS 260, 103 (DIK)
Draine B.T., 2003, ARA&A 41, 241
Egan M.P., Van Dyk S.D., Price S.D., 2001, AJ 122, 1844 (EDP)
Epchtein N., Deul E., Derriere S., et al., 1999, A&A 349, 236
Eyer L, 2002, AcA 52, 241
Feast M.W., Glass I.S., Whitelock P.A., Catchpole R.M., 1989, MNRAS 241, 375 (FGWC)
Feast M.W., Whitelock P.A., 1992, MNRAS 259, 6 (FW92)
Fluks M.A., Plez B., Thé P.S., et al., 1994, A&AS 105, 311
Frogel J.A., Blanco V.M., 1990, ApJ 365, 168 (FB90)
Frogel J.A., Mould J., Blanco V.M., 1990, ApJ 352, 96 (FMB)
Geha M., Alcock C., Allsman R.A., et al., 2003, AJ 125, 1
Glass I.S., 1979, MNRAS 186, 317
Glass I.S., 1986, MNRAS 221, 879
Glass I.S., Lloyd-Evans T., 1981, Nature 291, 303
Glass I.S., Lloyd-Evans T., 2003, MNRAS 343, 67 (GLE)
Glass I.S., Schultheis M., 2002, MN 337, 519
Glass I.S., Whitelock P.A., Catchpole R.M., Feast M.W., 1995, MNRAS 273, 383
Grison P., Beaulieu J.-P., Pritchard J. D., et al., 1995, A&AS 109, 447
Groenewegen M.A.T., 2004, in: "IAU Colloquium 193: Variable Stars in the Local Group", eds. D.W. Kurtz & Karen Pollard, ASP Conf. Ser., in press
Groenewegen M.A.T., Blommaert J.A.D.L., 1998, A&A 332, 25 (GB98)
Groenewegen M.A.T., Whitelock P.A., 1996, MNRAS 281, 1347
Hatzidimitriou D., Morgan D.H., Cannon R.D., Croke B.F.W., 2003, MNRAS 341, 1290 (HMCC)
Hughes S.M.G., 1989, AJ 97, 1634
Hughes S.M.G., Wood P.R., 1990, AJ 99, 784
Ita Y., Tanabé T., Matsunaga N., et al., 2004a, MNRAS 347, 720
Ita Y., Tanabé T., Matsunaga N., et al., 2004b, MNRAS in press (astro-ph/0312079)
Ita Y., 2004, in: "IAU Colloquium 193: Variable Stars in the Local Group", eds. D.W. Kurtz & Karen Pollard, ASP Conf. Ser., in press
Keller S.C., Bessell M.S., Cook K.H., Geha M., Syphers D., 2002, AJ 124, 2309
Kiss L.L., Bedding T., 2003, MNRAS 343, L79
Kiss L.L., Bedding T., 2004, MNRAS 347, L83
Kontizas E., Dapergolas A., Morgen D.H., Kontizas M., 2001, A&A 369, 932 (KDM)
Kunkel W.E., Irwin M.J., Demers S., 1997, A&AS 122, 463 (KID97)
Kunkel W.E., Demers S., Irwin M.J., 2000, AJ 119, 2789 (KDI00)
Lebzelter T., Schulteis M., Melchior A.L., 2002, A&A 393, 573
Loidl R., Lançon A., Jorgensen, U. G., 2001, A&A 371, 1065
Loup C., Cioni M.-R., Duc P.-A., Fouqué P., Groenewegen M.A.T., Azzopardi E., Habing H.J., 2003, A&A in preparation
Melchior A.-L., Hughes S.M.G, Guibert J., 2000, A&AS 145, 11
Mennickent R.E., Pietrzyński G., Gieren W., Szwewzyk O., 2002, A&A 393, 887
Mennickent R.E., Pietrzýnski G., Diaz M., Gieren W., 2003, A&A 399, L47
Meyssonnier N., Azzopardi M., 1993, A&AS 102, 451 (MA93)
Morgan D.H., Hatzidimitriou D., 1995, A&AS 113, 539 (MH)

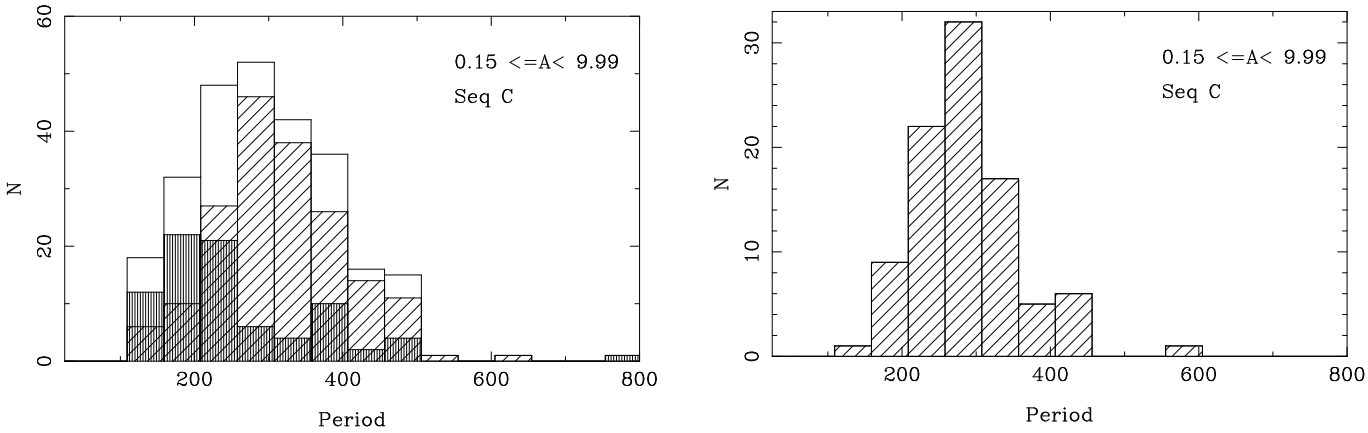

Fig. 16. Period distribution of the LMC (left panel) and SMC (right panel) variables in box "C" with I-band amplitudes larger than 0.15 magnitudes. Shown are the histograms for the M-stars (vertical lines), C-stars (hatched), and total.

Table 9. K-band PL-relations in box "C", of the form $m_{\rm K} = a \log P + b$

a	b	N	rms	remarks
-3.78 ± 0.24	20.17 ± 0.58	44	0.26	O-stars, LMC, Amplitude > 0.45 mag
-3.50 ± 0.27	19.42 ± 0.67	58	0.22	C-stars, LMC, Amplitude > 0.45 mag
-4.14 ± 0.85	21.34 ± 2.06	14	0.25	C-stars, SMC Amplitude > 0.45 mag
-3.52 ± 0.16	19.56 ± 0.38	83	0.26	O-stars, LMC, Amplitude > 0.15 mag
-3.56 ± 0.15	19.57 ± 0.38	181	0.25	C-stars, LMC, Amplitude > 0.15 mag
-3.67 ± 0.24	20.22 ± 0.60	92	0.24	C-stars, SMC, Amplitude > 0.15 mag
-3.47 ± 0.19	19.48 ± 0.45	29	0.13	M-Miras, LMC, FGWC
-3.52 ± 0.21	19.64 ± 0.49	26	0.13	M-Miras, LMC, GLE03
-3.30 ± 0.40	18.98 ± 0.98	20	0.18	C-Miras, LMC, FGWC
-3.56 ± 0.17	19.64 ± 0.42	54	0.25	C-Miras, LMC, Groenewegen & Whitelock (1996)

Munari U, Zwitter T., 2002, A&A 383, 188
Nishida S., Tananbe T., Nakada Y., et al., 2000, MNRAS 313, 136
Noda S., Takeuti M., Abe F., et al., 2002, MNRAS 330, 137
Olivier E.A., Wood P.R., 2003, ApJ 584, 1035
Prevot L., Martin N., Maurice E., Rebeirot E., Rousseeau J., 1983, A&AS 53, 255 (PMMR)
Rebeirot E., Azzopardi M., Westerlund B.E., 1993, A&AS 97, 603 (RAW)
Reid N., Glass I.S., Cathpole R.M., 1988, MNRAS 232, 33
Reid N., Hughes S.M.G., Glass I.S., 1995, MNRAS 275, 331
Reid N., Mould J., 1990, ApJ 360, 490 (RM90)
Richer H.B., 1981, ApJ 243, 744
Sanduleak N., 1989, AJ 98, 825 (SkKM)
Sebo K.M., Wood P.R., 1995, ApJ 449, 164
Smith V.V., Plez B., Lambert D.L., Lubowich D.A., 1995, ApJ 441, 735 (SPLL)
Soszyński I., Udalski A., Szymański M., et al., 2002, AcA 52, 369
Soszyński I., Udalski A., Szymański M., et al., 2003, AcA 53, 93
Sperl M., 1998, Comm. Astroseismology 111, 1
Lloyd Evans T., 1978a, MNRAS 183, 305 (TLE78a)
Lloyd Evans T., 1978b, MNRAS 183, 319 (TLE78b)
Lloyd Evans T., 1980, MNRAS 193, 87 (TLE80)
Trams N.R., Van Loon J.Th., Waters L.B.F.M., et al., 1999, A&A 346, 843 (T99)
Udalski A., Kubiak M., Szymański M., 1997, AcA 47, 319
Udalski A., Soszyński I., Szymański M., et al., 1998, AcA 45, 563
Udalski A., Soszyński I., Szymański M., et al., 1999a, AcA 49, 1
Udalski A., Soszyński I., Szymański M., et al., 1999b, AcA 49, 45
Udalski A., Soszyński I., Szymański M., et al., 1999c, AcA 49, 223
Udalski A., Soszyński I., Szymański M., et al., 1999d, AcA 49, 437
van Loon J.Th., Zijlstra A.A., Kaper L., et al., 2001, A&A 368, 239
Wagenhuber J., Groenewegen M.A.T., 1998, A&A 340, 183
Westerlund B.E., Olander N., Hedin B., 1981, A&AS 43, 267 (WOH)
Westerlund B.E., Azzopardi M., Breysacher J., Rebeirot E., 1991, A&AS 91, 425 (WABR91)
Westerlund B.E., Azzopardi M., Breysacher J., Rebeirot E., 1995, A&A 303, 107 (WABR95)
Whitelock P.A., Feast M.W., Menzies J.W., Catchpole R.M., 1989, MNRAS 238, 769
Whitelock P.A., Feast M.W., van Loon J.Th., Zijlstra A.A., 2003, MNRAS 342, 86 (WFLZ)
Wilke K., Stickel M., Haas M., et al., 2003, A&A 401, 873
Wood P.R., 1990, in: "From Miras to Planetary Nebulae", eds. M.O. Mennessier, A. Omont, Editions Frontieres, Gif-sur-Yvette, p. 67
Wood P.R., 1998, A&A 338, 592
Wood P.R., 2000, PASA 17, 18
Wood P.R., 2003, in: "Mass-lising pulsating stars and their circumsetallar matter", eds. Y. Nakada, M. Honma & M. Seki, Kluwer academic publishers, p. 3
Wood P.R., 2004, in: "IAU Colloquium 193: Variable Stars in the Local Group", eds. D.W. Kurtz & Karen Pollard, ASP Conf. Ser., in press
Wood P.R., Alcock C., Allsman R.A., et al., 1999, in: "IAU Symposium 191: AGB stars", eds. T. Le Bertre, A. Lèbre and C. Waelkens, Kluwer Academic Publishers, ASP, p. 151
Wood P.R., Bessell M.S., Fox M.W., 1983, ApJ 272, 99 (WBF)
Wood P.R., Bessell M.S., Paltoglou G., 1985, ApJ 290, 477 (WBP)
Wood P.R., Sebo K.M., 1996, MNRAS 282, 958

Wood P.R., Whiteoak J.B., Hughes S.M.G., et al., 1992, ApJ 397, 552
Wood P.R., Zarro D.M., 1981, ApJ 247, 247
Wyrzykowski L., Udalski A., Kubiak M., et al., 2003, AcA 53, 1
Zebruń K., Soszyński I., Woźniak P., et al., 2001, AcA 51, 317
Zijlstra A.A., Bedding T.R., 2003, JAVSO 31, 2
Zijlstra A.A., Bedding T.R., Mattei J.A., 2002, MNRAS 334, 498

Appendix A: Step 1: Fourier analysis and light curve fitting

At the heart of the first code are the NUMERICAL RECIPES subroutines *fasper* and *mrqmin* that perform a Fourier transformation and a (weighted) linear least-squares fitting, respectively. The function that is fitted to the data has the following form:

$$I(t) = I_0 + \sum_{i=1}^{i=n_{\rm max}} \Big(A_{\rm i} \sin(2\pi\ t\ e^{f_{\rm i}}) + B_{\rm i} \cos(2\pi\ t\ e^{f_{\rm i}}) \Big) \qquad \text{(A.1)}$$

This is a more suitable form for fitting purposes than the equivalent form (with $\omega = e^f$):

$$I(t) = I_0 + \sum_{i=1}^{i=n_{\rm max}} C_{\rm i} \sin(2\pi\ t\ \omega_{\rm i} + \phi_{\rm i})$$

Up to three periods are fitted ($n_{\rm max}$ = 3), following Wood et al. (1999). These two subroutines are called alternatingly, subtracting the best fit sofar from the data, and then performing a Fourier analysis on the residual. If a significant peak is found, a fit including the next term in the series in Eq. 1 is included. This is repeated until no significant peak in the power spectrum is found or the third period has been fitted.

The Fourier analysis is done with the subroutine *fasper*. Inputs to it are the time and magnitude arrays. In addition one has to specify two parameters, *ofac* and *hifac*, that indicate a "typical oversampling factor" and the maximum frequency in terms of a "typical" Nyquist frequency.

In the present work *ofac* = 22 and *hifac* = 0.8 are used. The latter parameter is the determining factor in both the computational speed, and the shortest period that can be found. For example, some tests to correctly identify the main period in an RR Lyrae object with a known period of 0.55 days required *hifac = 10.0*. In this configuration the code would be more than a factor of 10 slower. At the same time it implies that in the configuration used in the present paper there is a bias in the detection of periods shorter than about 6 days, of no consequence as the focus is on AGB stars.

The output of *fasper* are the frequency where the peak occurs and a number indicating a *significance*. One of the main parameters in the code is to provide the critical cut-off above which a period is not considered to be significant. In the present work *significance* = 5.5×10^{-11} is used, and this was determined empirically, by visually inspecting many lightcurves.

The code can be run in a single-star mode (for fine tuning) or in an automatic mode. It should be pointed out that some of the features and parameters just described and that will be described below have been determined only empirically. In fact, the cycle of Steps 1 and 2, and partly Step 3, has been repeated a few times to check the various steps in detail and come to the final choice of the parameters. The content of the code is now described in detail.

- Read in the files with 2MASS and DENIS objects that are within $3''$ of OGLE objects.
  Read in the file which contains the path names to the 68 000 files which contain the I-band data.
  The steps below are either done for one star (in single-star mode) or for all.
- Read in the path-name (e.g. smc_sc5/OGLE005013.32-731112.6.mag), and construct the right ascension and declination from it. Read in the individual Julian Dates, I-band magnitudes and errors. If there are less than 11 data points, exit. Otherwise enter the light curve fitting subroutine.
- Loop over the data points, and remove those with error "-99". Loop over the remaining data points and determine the largest time gap between two subsequent data points in time. If there are less than 30 data points or a time gap larger than 250 days, exit.
- Order the data points according to the error bar in the I-magnitude. Automatically reject 5% of the data with the largest errors. Order the data points according to the I-magnitude. Automatically reject the 3 brightest data points. This last step was introduced when it became clear that a few very bright (spurious ?) outliers in faint sources severely biased the light curve fitting because these outlying points carry so much weight. In bright sources this procedure has no bearing on the outcome. The final data arrays with time, I-magnitude and error in I-magnitude are constructed, and written to file, so that they can be read in by an independent time-analysis code (PERIOD98, Sperl 1998) in single-star mode.
- **I.** The best fit so far is subtracted from the data. At the first instance a constant is subtracted. The residual is inputted to *fasper*. If the significance of the peak is above the cut-off, or already $n_{\rm max}$ periods have been determined, goto **II.**
  In single-star mode the frequency sometimes has to be set to twice or half the frequency found by *fasper* at this stage in order to let the program converge to the correct result.
- First guesses for the amplitudes (see Eq. 1) are determined, and then the data plus parameters are inputed to *mrqmin*. At least two calls to *mrqmin* are made, and these calls are then repeated until subsequent χ^2 values agree to within 1% (or until a maximum of 10 iterations is reached). The χ^2 value is stored.
- For the improved fit, for each data point the deviation in terms of sigma is determined and if the data point with the largest deviation deviates more than 10σ from the fit, the error bar of that point is set to a very large value, so that that point is ignored in the further analysis.
- goto **I.**
- **II.** Plot the light curves including the best fit, and write all relevant output to file.
- Do the final correlation with DENIS and 2MASS using a search radius of $1.5''$. This takes into account the typical accuracy of the coordinates in the OGLE, DENIS and 2MASS surveys. Multiple matches are allowed for. The relevant data is written to file.

Appendix B: Step 2: Selecting AGB stars and general statistics

In the second code a preliminary list of LPV candidates is determined, by applying (if one wishes) selections in magnitude, periods and amplitudes and by eliminating known non-LPVs and correlating with known LPVs and/or AGB stars. These issues are discussed here.

B.1. Known sources

The advantage of compiling a list of variable objects in the direction of the MCs that are known not to be LPVs is twofold. First, it immediately limits the number of sources to be inspected visually in Step 3. Even more importantly, knowing the light curves of known non-LPVs helps identifying other such kind of objects in Step 3.

The literature was scanned for lists of objects identified in OGLE and other microlensing surveys MACHO, MOA, EROS in the direction

of the MCs (hence not restricted to the OGLE fields). Eclipsing binaries (EBs) were included from Udalski et al. (1998; OGLE, 1459 in SMC), Wyrzykowski et al. (2003; OGLE, 2580 in LMC), Alcock et al. (1997; MACHO, 637 in LMC), Bayne et al. (2002; MOA, 167 in SMC), Grison et al. (1995; EROS, 79 in LMC). RV Tau objects from Alcock et al. (1998; MACHO, 33 in LMC). R CrB stars from Alcock et al. (2001; MACHO, 17 in LMC). A few known and many new candidate QSO from Eyer (2002; OGLE, 133 in SMC plus LMC), and Geha et al. (2003; MACHO, 59 SMC + LMC). Blue variable objects (possibly related to the Be phenomenon) from Mennickent et al. (2002; OGLE, 1056 in SMC), Mennickent et al. (2003; OGLE, 30 in SMC plus LMC), Eyer (2002; OGLE, 36 in SMC plus LMC), Keller et al. (2002; MACHO, 1280 in LMC). RR Lyrae stars from Soszyński et al. (2002, OGLE, 556 in SMC; 2003, 7612 in LMC) and Alcock et al. (2000; MACHO, 283 in LMC). Finally, Cepheids from Afonso et al. (2003; EROS, 880 in SMC and LMC), second overtone (SO) cepheids from Alcock et al. (1999; MACHO, 47 in LMC) and fundamental mode (FU), first overtone (FO), SO and double-mode (FU/FO and FO/SO) cepheids from Udalksi et al. (1999a,b,c,d; OGLE, 3492 in SMC + LMC).

This amounts to a total of 20863 objects (including double entries coming from different sources).

In Step 3 the SIMBAD database is queried and so previous observations will normally be identified in this way. On the other hand, not all (recent) data is yet included there. Therefore a list of known or suspected LPVs, mostly from recent large survey work, was compiled.

Two of the largest 'old' surveys for LPVs are those by Hughes (1989) and Reid, Hughes and Glass (1995). I was not able to trace the relevant tables in these papers in computer readable form, but through P. Wood I obtained a table originally prepared by S. Hughes that seems to combine the data from these two papers. Eliminating double entries it contains information on 1317 LPVs in the LMC (I will refer to this list as the Hughes-list from now on).

From the MOA survey the 146 LPVs in the LMC discussed by Noda et al. (2002) are considered.

M. Schultheis kindly made available the unpublished periods, amplitudes, magnitudes of the about 470 LPVs in the LMC bar discovered by the AGAPEROS survey and discussed in detail by Lebzelter et al. (2002)

From Cioni et al. (2003) the 458 objects in the SMC are considered that have been detected in a mini-survey with ISOCAM (Loup et al. 2004, in prep.), have reliable DENIS and 2MASS counterparts (in the 2nd incremental data release) and have a MACHO lightcurve.

P. Wood kindly made available the MACHO id numbers, coordinates, periods and photometry of the 1560 objects he studied in Wood et al. (1999) and Wood (2000) in the bar of the LMC.

From Feast et al. (1989), using additional information provided in Glass & Lloyd-Evans (2003) and references therein, 58 LMC objects are considered that *de facto* have been defined the Mira PL-relation.

Finally, a list of 45 IRAS sources was compiled from Wood et al. (1992), Wood (1998), Whitelock et al. (2003), that have been monitored in the infrared and were found to have well determined periods.

The total list of known LPVs contains 4053 objects.

In addition a list of spectroscopically confirmed M-, S-, and C-stars and supergiants with accurate coordinates (listed to $1''$ or better) was compiled from lists in Westerlund et al. (1981; WOH), Prevot et al. (1983; PMMR), Wood et al. (1985; WBP), Sanduleak (1989; SkKM), Reiberot et al. (1993; RAW), Kontizas et al. (2001; KDM), Morgan & Hatzidimitriou (1995; MH), Demers et al. (1993), Kunkel et al. (1997), Groenewegen & Blommaert (1998; GB98), Kunkel et al. (2000), Loup et al. (2003, specifically dealing with the Blanco fields as discussed in Blanco et al. (1980; BMB) and Frogel & Blanco 1990) and Cioni et al. (2001), for a total of 13175 stars (including some double-entries).

As for some of the stars in the Hughes-list a spectral type has been determined, in fact 13451 stars (including double entries) in this list have a spectral type assigned. Correlating this list with itself, using a $4''$ search radius, reveals 12631 unique entries (2899 C, 19 M, 0 S in the SMC, 8117 C, 1580 M, 16 S in the LMC). This list is strongly biased towards carbon stars because of the very large surveys in both LMC and SMC (notably RAW and KDM), and the lack of similar surveys for M-stars.

B.2. Cuts in magnitude, amplitude and period

In the present paper no cuts on magnitude, amplitude or period have been made, as the sample discussed below will be restricted to spectroscopically confirmed M-, S-, C-stars. For reference, in Groenewegen (2004) the following cuts were applied to the SMC data to select the LPV candidates: mean OGLE $I < 16.8$ mag, any of the fitted periods > 50 days, and any of the fitted amplitudes (in the classical sense, $C_i = \sqrt{A_i^2 + B_i^2}$ from Eq. 1) > 0.05 mag.

In hindsight, it would have been preferable to have had a faint limit (maybe at $I \sim$ 18-18.5) imposed as quite a few spectroscopically confirmed M,S,C-stars were positionally matched with very faint (mean $I \gtrsim$19) OGLE objects which were often barely variable, and clearly not the counterpart of the late-type stars.

B.3. More details

The content of the code is now described in detail.

- Read in the output file of Step 1, and the files with the coordinates of the known non-LPVs, and the known LPVs and spectroscopically confirmed M-,S-,C-stars.
- Only periods with an accuracy better than 2% are retained.
- The selection on mean I-magnitude, amplitude and period may be carried out. In the present paper no cuts have been applied.
- Objects that appear twice in different OGLE fields are identified and the one with the lowest χ^2 as determined in Step 1 is retained.
- The remaining objects are correlated on position (search radius $2''$) with the known non-LPVs. The identifiers of both the known non-LPVs and the remaining objects are written to file. This separation assumes that the classification in the literature of an object as Cepheid, RR Lyrae, eclipsing binary, etc, is correct.
- The remaining objects are correlated on position (search radius $4''$) with the known LPVs and spectroscopically confirmed M-,S-,C-stars. The identifiers of the cross-correlated objects are written to file in Latex format.
  In fact, to allow for small differences in the astrometry, corrections have been determined and applied, as discussed later.
- Independent of the selection of potential LPVs, in the second part of the code, general properties are investigated, like the positional match between OGLE and 2MASS, and OGLE and DENIS sources, and the difference between $I_{\rm ogle}$ and $I_{\rm denis}$, $J_{\rm 2mass}$ and $J_{\rm denis}$, and $K_{\rm 2mass}$ and $K_{\rm denis}$.

Appendix C: Step 3: Visual inspection and literature study

This last step is time consuming and involves several checks.

- A visual inspection of the fit to the data. If needed the fit is re-done with the code in single-star mode, and usually involves "twisting"

the first frequency it finds to half or twice its value. On some occasions the data is analysed with an independent code, PERIOD98 (Sperl 1998).
– Cross-correlation with the SIMBAD database. The coordinate list with candidate LPVs is send to the batch queue server of SIMBAD.
– Checking and completing of automatically generated tabular material in Latex format.

This figure "fig1.jpg" is available in "jpg" format from:

http://arXiv.org/ps/astro-ph/0404561v1

This figure "fig2.jpg" is available in "jpg" format from:

http://arXiv.org/ps/astro-ph/0404561v1

This figure "fig9.jpg" is available in "jpg" format from:

http://arXiv.org/ps/astro-ph/0404561v1


This figure "fig13.jpg" is available in "jpg" format from:
http://arXiv.org/ps/astro-ph/0404561v1